The termal circuits of the Argentera Massif (western Alps, Italy) : an example of low-enthalpy geothermal resources controlled by Neogene alpine tectonics

Autor(en): **Perello, Paolo / Marini, Luigi / Martinotti, Giorgio**

Objekttyp: **Article**

Zeitschrift: **Eclogae Geologicae Helvetiae**

Band (Jahr): **94 (2001)**

Heft 1

Persistenter Link: https://doi.org/10.5169/seals-168878

0012-9402/01/010075-20 $1.50 + 0.20/0
Birkhäuser Verlag, Basel, 2001

Eclogae geol. Helv. 94 (2001) 75–94

The thermal circuits of the Argentera Massif (western Alps, Italy): An example of low-enthalpy geothermal resources controlled by Neogene alpine tectonics

PAOLO PERELLO[1], LUIGI MARINI[2], GIORGIO MARTINOTTI[3] & JOHANNES C. HUNZIKER[4]

Key words: Argentera Massif, Western Alps, thermal water, low-enthalpy geothermal resource, brittle tectonic

ABSTRACT

This work presents geochemistry and structural geology data concerning the low enthalpy geothermal circuits of the Argentera crystalline Massif in northwestern Italian Alps.

In this area some thermal springs (50–60°C), located in the small Bagni di Vinadio village, discharge mixtures made up of a Na-Cl end-member and a Na-SO_4 component. The latter is also discharged by the thermal springs of Terme di Valdieri located some kilometres apart within the same tectonic complex. Both end-members share the same meteoric origin and the same reservoir temperature, which is close to 150°C. Explanations are thus required to understand how they reach the surface and how waters of the same origin and circulating in similar rocks can attain such different compositions.

Sodium-sulphate waters discharged at both sites, likely represent the common interaction product of meteoric waters with the widespread granitic-migmatitic rocks of the Argentera Massif, whereas Na-Cl waters originate through leaching of mineralised cataclastic rocks, which are rich in phyllosilicatic minerals and fluid inclusions, both acting as Cl^- sources.

Due to the relatively low inferred geothermal gradient of the region, ~25°C/km, meteoric waters have to descend to depths of 5.5–6 km to attain temperatures of ~150°C. These relevant depths can be reached by descending meteoric waters, due to the recent extensional stress field, which allows the development of geothermal circulations at greater depths than in other sectors of the Alps by favouring a greater fractures aperture. The ascent of the thermal waters takes place along brittle shear zones. In both sites, the thermal waters emerge at the bottoms of the valleys, close to either the lateral termination of a brittle shear zone at Terme di Valdieri, or a step-over between two en-echelon brittle shear zones at Bagni di Vinadio. These observations attest to a strong control operated on the location of outlet regions by both brittle tectonics and the minima in hydraulic potential inside the fractured massif.

RIASSUNTO

Questo studio riporta una caratterizzazione geochimica e geologico strutturale dei circuiti geotermici a bassa entalpia presenti all'interno del Massiccio cristallino dell'Argentera, nelle Alpi italiane nord-occidentali. In quest'area, alcune sorgenti termali (50–60°C), situate in prossimità dell'abitato di Bagni di Vinadio, scaricano delle acque che rappresentano miscele costituite da un end-member a composizione cloruro-sodica (Na-Cl) e da un end-member a composizione solfato-sodica (Na-SO_4). Quest'ultimo end-member è anche scaricato dalle sorgenti termali di Terme di Valdieri, localizzate ad alcuni chilometri di distanza dalle precedenti all'interno dello stesso complesso tettonico. Entrambi gli end-members mostrano una comune origine da acque meteoriche e la stessa temperatura di riequilibrazione, prossima a 150°C. Sono dunque necessarie delle spiegazioni per comprendere come essi raggiungano la superficie e come acque della stessa origine, che circolano in rocce simili possano raggiungere composizioni finali tanto diverse.

Le acque solfato sodiche, scaricate in entrambi i siti rappresentano probabilmente il risultato comune dell'interazione con le diffuse rocce granitiche e migmatitiche del Massiccio dell'Argentera, mentre le acque cloruro-sodiche traggono origine dalla lisciviazione di rocce di faglia mineralizzate, ricche in minerali fillosilicatici e in inclusioni fluide che agiscono entrambi come sorgenti di Cl^-.

A Causa del basso gradiente geotermico ipotizzabile per la regione, circa 25°C, le acque meteoriche devono infiltrarsi fino a profondità di 5.5–6 Km per raggiungere temperature di 150°C. Il presente studio ha permesso di concludere che tali considerevoli profondità possono essere raggiunte dalle acque meteoriche discendenti grazie alla presenza di un campo degli sforzi recente di tipo estensionale, che consente lo sviluppo di circolazioni consistenti a profondità maggiori che in altri settori delle Alpi favorendo una maggior apertura delle fratture. La risalita delle acque termali avviene lungo zone di taglio fragili. In entrambi i siti le acque termali vengono a giorno lungo dei fondivalle, in prossimità di terminazioni laterali di zone di deformazione fragili (Terme di Valdieri), o in prossimità di zone di ponte tra due zone di taglio fragili en-echelon (Bagni di Vinadio). Queste osservazioni testimoniano un forte controllo operato sull'ubicazione delle zone di emergenza da parte sia degli elementi tettonici recenti che dei minimi di potenziale idraulico all'interno del massiccio fratturato.

[1] SEA Consulting s.r.l., Via Gioberti 78, I–10128 Torino, Italy. E-mail: perello@seaconsult.it
[2] Department of Earth Sciences, University of Genova, Corso Europa 26, I–16132 Genova, Italy. E-mail: luigi@ugo.dister.unige.it
[3] Department of Earth Sciences, University of Torino, Via Valperga Caluso 37, I–10125 Torino, Italy. E-mail: martinotti@dst.unito.it
[4] Institut de Minéralogie et Pétrographie, Université de Lausanne, BFSH-2, CH–1015 Lausanne, Switzerland. E-mail: johannes.hunziker@imp.unil.ch

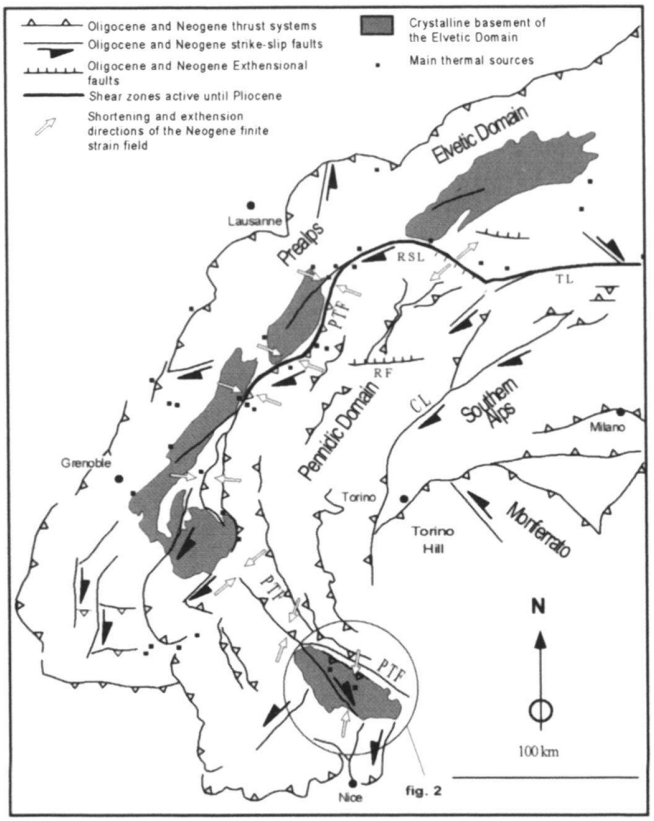

Fig. 1. Tectonic sketch map of the Western Alps. Dark shadowed areas are the External crystalline Massifs (European continental crust). Dots are the most important thermal springs. RSL = Rhone-Simplon Line, TL = Tonale Line, PTF = Penninic Thrust Front, RF = Ranzola Fault.

1. Introduction

Low-enthalpy geothermal resources are widespread in the central and western Alps. They are mainly represented by thermal springs and by water inflows in deep tunnels, with flow rates of 0.1–50 kg/s and temperatures of 20–70°C (Vuataz 1982; Rybach 1995; Perello 1997).

Chemical and isotopic composition of these thermal waters indicate that they are meteoric waters heated through conductive heat transfer from hot rocks at depth, in areas of geothermal gradient either normal or slightly higher than normal.

In spite of the abundant information on the chemical and isotopic composition of the alpine thermal waters, very little work has been done in the past to understand the lithological and tectonic constraints controlling their localisation, even though the simple geographical distribution of thermal waters suggests a likely control by important late-alpine (Neogene) brittle shear zones (Fig.1). Many thermal water discharges are located, in fact, close to the Penninic Front, a ductile deformation zone reactivated by brittle shearing during late Neogene (Hubbard & Mancktelow 1992; Laubscher 1991; Perello et al. 1999; Seward & Mancktelow 1994). Other thermal springs are located in the Lepontine Dome, a region characterised by a geothermal gradient slightly higher than normal for the Alps (30–35°C compared to the normal gradient of 20–25°C; Clark & Niblett 1956) and are probably related to uplift induced by recent tectonic activity which took place along the Rhone-Simplon shear zone (Mancktelow 1985; Steck 1990; Steck & Hunziker 1994). Finally, widespread occurrences are present in the external Alps, in relation with important Neogene tectonic features like the Jura Front.

The present work deals with the case of two thermal water discharges, Terme di Valdieri and Bagni di Vinadio (in the following mainly abbreviated to Valdieri and Vinadio), which are located approximately 17 km apart, within the Argentera Massif (AM). Alpine structures are relatively well known in the south-western sector of the AM (Bogdanoff 1986; Guardia & Ivaldi 1985). Conversely they were poorly studied in the other sectors, including the areas of Bagni di Vinadio and Terme di Valdieri, which were therefore surveyed together with the Demonte-Valdieri area in the framework of the present investigation (Fig. 2, Pl. 1, Pl. 2 and Pl. 3). Detailed structural mapping was carried out in these areas, to investigate the geological constraints possibly controlling the localisation of thermal water discharges and to get some insight into the extension at depth of the water circuits feeding these thermal springs.

Both at Valdieri and at Vinadio, thermal waters are discharged by several springs, which are located within small areas of 10,000 m^2 approximately (Pl.2 and 3). Maximum outlet temperatures are close to 60°C. Although the geochemistry of the Terme di Valdieri and Bagni di Vinadio thermal waters is relatively well-known (Fancelli & Nuti 1978; Bortolami et al. 1984; Michard et al. 1989), 27 samples of thermal discharges and cold waters were collected and analysed both chemically and isotopically (Tab. 1), following similar field and laboratory techniques as Pastorelli et al. (1999).

This study is part of a broader investigation aimed at the evaluation and interpretation of thermal occurrences in the Alpine chain.

2. Geological setting

The AM is a structural high of the European plate crystalline basement (Fig. 1). This basement crops out owing to its uplift and to the subsequent erosion of the overlying Mesozoic sedimentary succession (Helvetic-Dauphinois cover, HDC). The AM mainly consists of two gneissic complexes, known as the Malinvern-Argentera Complex and the Tinée Complex (Fig. 2). They are separated by a steep, NW-SE striking mylonite belt, which is known as the Ferriere-Mollières line (or FM line, Malaroda et al. 1970). This pre-alpine structural element was reactivated by ductile and brittle deformation in alpine age.

The Malinvern-Argentera Complex is mainly composed of migmatitic gneisses related to pre-alpine, high-grade metamorphism of both para- and ortho-derived protolithes (Bogdanoff 1986). The mineralogical components of these gneisses are

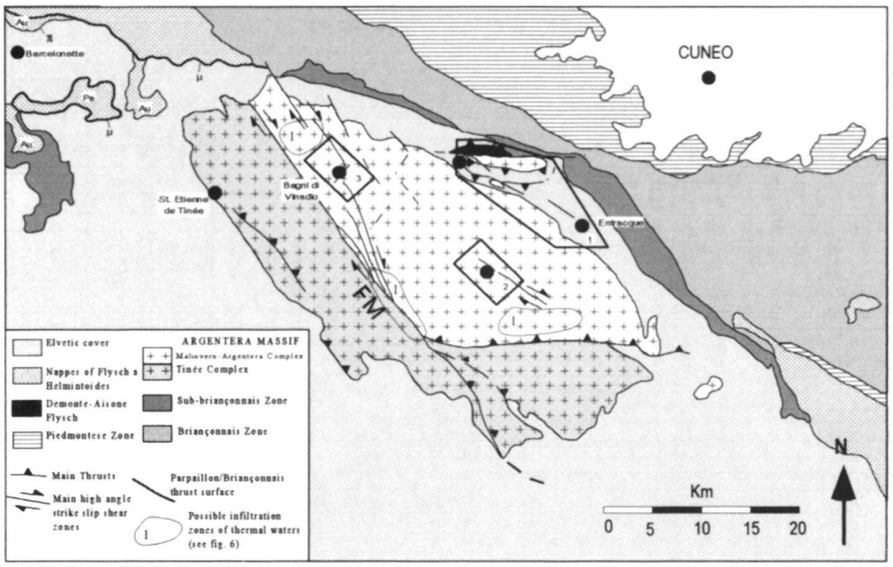

Fig. 2. Sketch map of the Argentera Massif and adjoining regions; π = Subbriançonnais/Autapie Thrust Surface, μ = Parpaillon/Briançonnais Thrust Surface, FM = Ferriere-Mollieres Line, Au = Autapie Nappe, Pa = Parpaillon Nappe; 1, 2, 3 = areas studied in detail and represented in Plates 1, 2, 3.

quartz, K-feldspar, plagioclase, biotite, and minor muscovite and sillimanite (Malaroda et al. 1970). High-grade gneisses are intruded by syn-anatectic, leucocratic, meta-granites and by late Hercynian meta-granites (Ferrara & Malaroda 1969 Compagnoni et al. 1974).

The Tinée Complex is similar to the Malinvern-Argentera Complex in that it mainly consists of anatectic gneisses derived partly from sedimentary and partly from plutonic protoliths (Bogdanoff 1986).

The gneisses of the AM show a pervasive composite schistosity developed in pre-alpine age during different stages of high-grade metamorphism and deformation (Bogdanoff 1986). The FM line, which separates the two complexes, is probably related to a late pre-alpine deformation event (Bogdanoff 1986).

The meta-sedimentary cover of the AM (HDC) crops out in a belt around the basement (Fig. 2). It can be subdivided in an autocthonous succession of Carboniferous-Triassic age, which is represented by continental sediments (conglomerates, volcanoclastic deposits, pelites, quartzites) and a detached succession of post-middle Triassic age (Faure-Muret 1955; Sturani 1962; Malaroda et al. 1970). The detachment surface is marked by middle Triassic evaporites (cargneules). Despite local sedimentary variations, the detached Mesozoic succession mainly consists of dolostones, limestones, schists and meta-arenites of Triassic-Oligocene age (Sturani 1963; Malaroda et al. 1970). The HDC, together with the AM, was subjected to anchimetamorphic and locally epimetamorphic conditions in alpine times.

Both the massif and its cover are locally affected by a more or less pervasive hydrothermal alteration (see paragraph 4). At present, the thermal waters discharge at the surface inside the Malinvern-Argentera Complex (Fig. 2). Nevertheless the abundant traces of past hydrothermal activity attest that it has been a diffuse and repeated phenomenon during all the alpine deformation history of the AM region.

3. Fluid geochemistry

3.1. Isotopic characteristics of the thermal waters

In the classic δD vs. $\delta^{18}O$ plot (Fig. 3.1) the thermal discharges of both sites and the local cold waters lie close to the world-wide meteoric water line (Rozanski et al. 1993):

$$\delta D = (8.17 \pm 0.06) \cdot \delta^{18}O + (10.35 \pm 0.65). \qquad (1)$$

All the thermal springs, except one from Valdieri, and all the cold waters are slightly shifted towards higher δD or lower $\delta^{18}O$, possibly due to the influence of Mediterranean precipitations (Dazy et al. 1987). Vinadio and Valdieri thermal waters do not exhibit positive ^{18}O-shifts, which are typical of high-temperature geothermal systems and are larger in essentially stagnant rock-dominated systems than in dynamic, fluid-dominated systems (Giggenbach 1992). This lack of ^{18}O-shifts in the waters of the study area agrees with their provenance from possibly dynamic geothermal systems of comparatively low temperature (~115°C according to Michard et al. 1989; ~150°C according to the Na-K-$Mg^{1/2}$ triangular plot, see below). The δD and $\delta^{18}O$ values of Vinadio are slightly more negative than those of Valdieri, indicating a small difference in the elevations of the infiltration areas of the meteoric waters feeding the two thermal circuits. These are probably in the range 1800–2100 m asl (Fancelli & Nuti 1978; Michard et al. 1989), although Bortolami et al. (1984) proposed an infiltration altitude of ~1400 m asl for Valdieri, hypothesising an unrealistic occurrence of

Table 1. Geochemical and isotopic data from springs of the study area. Locations of sources are reported in Plates 1 and 2. (*) Data from Fancelli & Nuti (1978); (**) Data from Michard et al. (1989). The source SD comes from the cover of the Argentera Massif outside of the mapped area.

Locality	code	sampling date	T °C	pH	Li mg/L	Na mg/L	K mg/L	Mg mg/L	Ca mg/L	Alkalinity mg/L(HCO3)	Carbonate Alk.	SO4 mg/L	Cl mg/L	F mg/L	SiO2 mg/L	B mg/L	δD per mil	δ18O per mil
Bagni di Vinadio	1a	(*)	46.7	8.47	1.96	582	28.4	0.19	55.3	34.8	25.0	28.8	1030	10.2	51.7	0.78	n.a.	-13.1
Bagni di Vinadio	1c	(*)	30.7	8.82	1.37	428	19.7	0.073	30.7	33.0	16.7	28.8	713	10.7	51.5	0.55	n.a.	-13.0
Bagni di Vinadio	1d	(*)	50.5	8.45	2.01	591	28.0	0.18	57.7	28.1	17.9	26.9	1020	10.2	52.4	0.80	-88.0	-12.8
Bagni di Vinadio	1e	(*)	52.5	8.28	2.15	655	29.7	0.19	61.3	26.2	18.7	30.7	1080	10.2	51.4	0.87	n.a.	n.a.
Bagni di Vinadio	2a	(*)	55.0	8.87	0.69	226	11.5	0.013	6.7	68.3	17.6	33.6	301	13.8	73.0	0.28	-91.7	-12.8
Bagni di Vinadio	2b	(*)	55.6	8.51	0.67	228	11.3	0.058	6.4	87.9	66.8	28.8	266	14.6	77.6	0.26	-89.0	-12.9
Bagni di Vinadio	1a	(**)	44.6	8.35	n.a.	537	35.0	0.30	55.0	46.8	n.c.	58.0	956	n.a.	49.0	n.a.	n.a.	-13.1
Bagni di Vinadio	1b	(**)	50.0	7.80	n.a.	635	39.0	0.40	63.0	190	n.c.	63.0	1060	n.a.	47.0	n.a.	n.a.	-13.3
Bagni di Vinadio	1c	(**)	24.2	7.70	n.a.	348	21.0	0.10	23.0	20.3	n.c.	70.0	601	n.a.	43.0	n.a.	n.a.	-13.0
Bagni di Vinadio	2a	(**)	54.9	8.90	n.a.	208	13.0	0.10	5.0	48.8	n.c.	41.0	319	n.a.	72.0	n.a.	n.a.	-13.0
Bagni di Vinadio	2b	(**)	50.7	9.05	n.a.	179	13.0	0.10	3.0	22.4	n.c.	55.0	267	n.a.	76.0	n.a.	n.a.	-13.3
Bagni di Vinadio	V1	04.06.96	54.4	9.05	0.80	212	13.9	0.037	10.0	38.0	4.2	56.1	315	13.6	69.5	n.a.	n.a.	n.a.
Bagni di Vinadio	V2	05.06.96	44.1	8.56	2.30	586	34.5	0.20	63.4	30.5	20.6	40.1	1040	12.1	52.5	n.a.	n.a.	n.a.
Bagni di Vinadio	V3	05.06.96	52.3	8.55	2.50	615	36.7	0.26	70.9	31.7	20.1	39.5	1130	10.7	49.5	n.a.	n.a.	n.a.
Bagni di Vinadio	V4	05.06.96	39.2	8.73	2.29	592	33.4	0.25	64.9	31.7	20.0	37.4	1040	11.9	49.9	n.a.	n.a.	n.a.
Bagni di Vinadio	V5	05.06.96	50.8	9.12	0.38	104	6.3	0.13	7.1	48.8	16.3	44.2	115	12.5	62.2	n.a.	n.a.	n.a.
Bagni di Vinadio	V6	05.06.96	53.9	8.88	0.73	196	12.7	0.08	8.9	50.0	22.3	40.5	282	14.1	73.1	n.a.	n.a.	n.a.
Bagni di Vinadio	V7	05.06.96	51.4	8.32	3.17	765	50.8	0.40	89.3	30.5	22.7	39.2	1430	9.9	54.4	n.a.	n.a.	n.a.
Pozzo terme	V8	05.06.96	5.5	7.31	n.a.	1.1	0.82	0.60	9.9	31.7	31.7	5.9	0.4	n.a.	4.9	n.a.	n.a.	n.a.
Terme di Valdieri	2	(*)	60.5	9.19	0.17	72.2	4.2	0.024	4.9	58.0	7.6	61.5	33.3	11.9	67.3	0.082	-84.9	-12.4
Terme di Valdieri	3	(*)	60.3	9.20	0.18	75.9	4.3	0.061	4.9	59.2	6.5	57.6	28.4	12.3	69.7	0.078	-85.4	-12.2
Terme di Valdieri	4	(*)	56.1	9.23	0.22	82.5	3.7	0.005	4.0	65.9	10.2	62.4	31.9	13.3	73.9	0.099	-86.7	-12.4
Terme di Valdieri	5c	(*)	31.6	9.57	0.22	82.1	3.9	0.058	4.0	63.5	11.5	65.3	31.9	13.3	73.3	0.25	-88.0	-12.3
Terme di Valdieri	2	(**)	59.9	8.00	n.a.	72.5	2.5	n.d.	5.8	40.7	n.c.	62.4	32.0	n.a.	61.5	n.a.	n.a.	n.a.
Terme di Valdieri	3b	(**)	48.3	8.30	n.a.	67.0	2.4	0.10	7.7	41.7	n.c.	59.0	27.0	n.a.	55.5	n.a.	n.a.	-12.5
Terme di Valdieri	3d	(**)	60.2	9.50	n.a.	74.0	2.7	0.20	6.0	41.7	n.c.	65.0	30.0	n.a.	63.0	n.a.	n.a.	-12.4
Terme di Valdieri	4	(**)	55.6	9.60	n.a.	82.0	3.6	0.40	5.0	50.3	n.c.	63.0	34.0	n.a.	62.0	n.a.	n.a.	-12.8
Terme di Valdieri	S1	04.06.96	30.1	8.97	0.06	22.7	2.2	1.04	15.0	61.0	49.0	29.6	7.8	3.2	38.1	n.a.	n.a.	n.a.
Terme di Valdieri	S1	30.10.95	31.7	8.70	0.06	18.5	2.3	0.97	18.3	61.0	54.7	30.4	6.6	3.2	28.4	n.a.	-81.4	-11.0
Terme di Valdieri	S2	04.06.96	56.5	9.30	0.20	74.8	3.6	0.03	6.5	72.6	19.7	61.1	26.1	12	70.6	n.a.	n.a.	n.a.
Terme di Valdieri	S2	30.10.95	57.0	8.62	0.23	63.6	3.7	0.01	5.6	61.0	20.4	62.4	25.5	11.8	72.5	n.a.	n.a.	n.a.
Terme di Valdieri	S3	04.06.96	58.5	9.20	0.20	75.3	3.8	0.047	6.1	69.5	22.8	67.2	26.4	11.6	67.7	n.a.	n.a.	n.a.
Terme di Valdieri	S3	30.10.95	60.0	9.28	0.23	64.9	3.7	0.01	5.9	45.8	13.4	64.9	25.8	11.7	74.0	n.a.	n.a.	-12.3
Terme di Valdieri	S4	04.06.96	32.8	9.63	0.23	79.8	3.9	0.10	5.8	61.0	14.4	71.8	30.0	12.1	66.2	n.a.	n.a.	n.a.
Terme di Valdieri	S4	30.10.95	33.6	9.52	0.25	70.0	3.9	0.01	5.8	57.0	11.0	70.0	29.1	12.1	77.2	n.a.	-85.5	-12.3
Terme di Valdieri	S5	04.06.96	19.0	8.20	0.14	55.9	2.5	0.44	7.3	59.7	58.6	51.3	19.8	8.3	46.1	n.a.	n.a.	n.a.
Terme di Valdieri	S5	30.10.95	21.2	8.12	0.17	57.6	3.0	0.15	8.0	49.4	48.7	61.2	21.9	10.2	42.9	n.a.	n.a.	n.a.
Terme di Valdieri	S6	31.10.95	43.6	9.19	0.22	69.3	3.9	0.02	6.1	62.8	33.0	72.5	26.4	11.8	55.4	n.a.	n.a.	n.a.
Terme di Valdieri	S7	04.06.96	49.5	9.37	0.20	73.7	3.7	0.053	7.4	62.2	14.6	68.4	26.0	11.7	66.9	n.a.	n.a.	n.a.
Terme di Valdieri	S7	31.10.95	51.0	9.12	0.20	67.5	3.7	0.006	8.7	59.8	20.7	70.1	25.3	11.6	77.3	n.a.	n.a.	n.a.
Acqua fredda	AF	(**)	n.a.	8.20	n.a.	1.0	0.30	1	7.0	10.1	10.1	7.0	n.d.	n.a.	20.0	n.a.	n.a.	-13.0
Combal Jors	CJ	(**)	10.3	7.00	n.a.	5.0	0.90	2	9.0	19.0	19.0	19.0	4.0	n.a.	11.0	n.a.	n.a.	-12.9
Ciriegia	Ci	(**)	15.0	7.20	n.a.	5.0	0.70	0.20	20.9	54.0	54.0	17.5	2.0	n.a.	9.0	n.a.	n.a.	n.a.
Tumpi	Tm	(**)	8.6	6.90	n.a.	1.3	1.80	0.30	7.2	15.4	15.4	5.3	4.2	n.a.	4.0	n.a.	n.a.	-12.2
Valdieri	SD		8.5	7.84	n.a.	1.6	0.75	23.5	112	88.4	88.4	288	1.4	0.13	7.1	n.a.	n.a.	n.a.
Valdieri	S8	04.06.96	5.5	7.06	n.a.	1.1	0.51	0.44	6.6	19.0	19.0	4.8	0.3	n.a.	5.2	n.a.	n.a.	n.a.
Valdieri	S8	31.10.95	9.1	6.82	0.01	1.0	0.58	0.56	8.1	22.8	22.8	5.0	0.9	0.07	6.0	n.a.	-77.1	-11.1
Valdieri	S9	31.10.95	12.4	6.85	n.a.	4.5	0.80	0.52	8.7	22.8	22.8	9.1	1.9	0.63	10.3	n.a.	n.a.	-12.0
Valdieri	S9	04.06.96	8.5	6.58	0.01	3.5	0.66	0.57	7.4	24.0	24.0	7.3	1.1	0.48	7.7	n.a.	n.a.	n.a.
Torrente Corborant	Co	05.06.96	6.6	7.94	n.a.	0.9	0.24	0.35	6.6	20.0	20.0	4.4	0.3	n.a.	3.9	n.a.	n.a.	n.a.
Torrente Gesso	Ge	31.10.95	5.9	7.45	0.01	0.9	0.36	0.26	6.5	15.8	15.8	4.0	1.0	0.17	4.9	n.a.	-76.5	-11.0

steam separation during the ascent of the thermal waters towards the surface.

Available tritium data (Fancelli & Nuti 1978; Bortolami et al. 1984; Michard et al. 1989) referred to 1989 are 0 to 0.8 TU at Vinadio (8 measurements) and 1 to 4.3 TU at Valdieri (6 data). The mean residence time, τ, of these waters can be roughly evaluated considering the ^3H data in local precipitations and referring to the two theoretical models of piston flow and perfect-mixing (Pearson and Truesdell 1978). According to the first model, τ is greater than some tens of years at both sites, whereas based on the perfect-mixing model, τ is of ~1000 to several thousand years at Valdieri and greater than several thousands years at Vinadio. Since fluid residence time in natural systems is likely intermediate between these two theoretical models, circulation times might be greater at Vinadio than at Valdieri. In any event, all these thermal waters should have τ values sufficiently large to allow attainment of mineral-solution thermochemical equilibrium at depth.

3.2. *Water chemistry*

Both the Valdieri and Vinadio thermal waters have pH values of 8–9 or even higher. Valdieri waters have total alkalinities of 0.31–1.20 meq/kg. Contrary to what is observed in most natural waters, whose total alkalinity and carbonate alkalinity are virtually indistinguishable, the carbonate alkalinities of Valdieri waters (obtained through speciation calculations carried out by means of SOLVEQ, Reed & Spycher 1984) are 0.11–0.97 meq/kg only. The difference between total alkalinity and carbonate alkalinity of Valdieri waters is due to their high pH values, causing high concentrations of $H_3SiO_4^-$, OH^-, HS^- and other ions contributing to total alkalinity. For instance, the

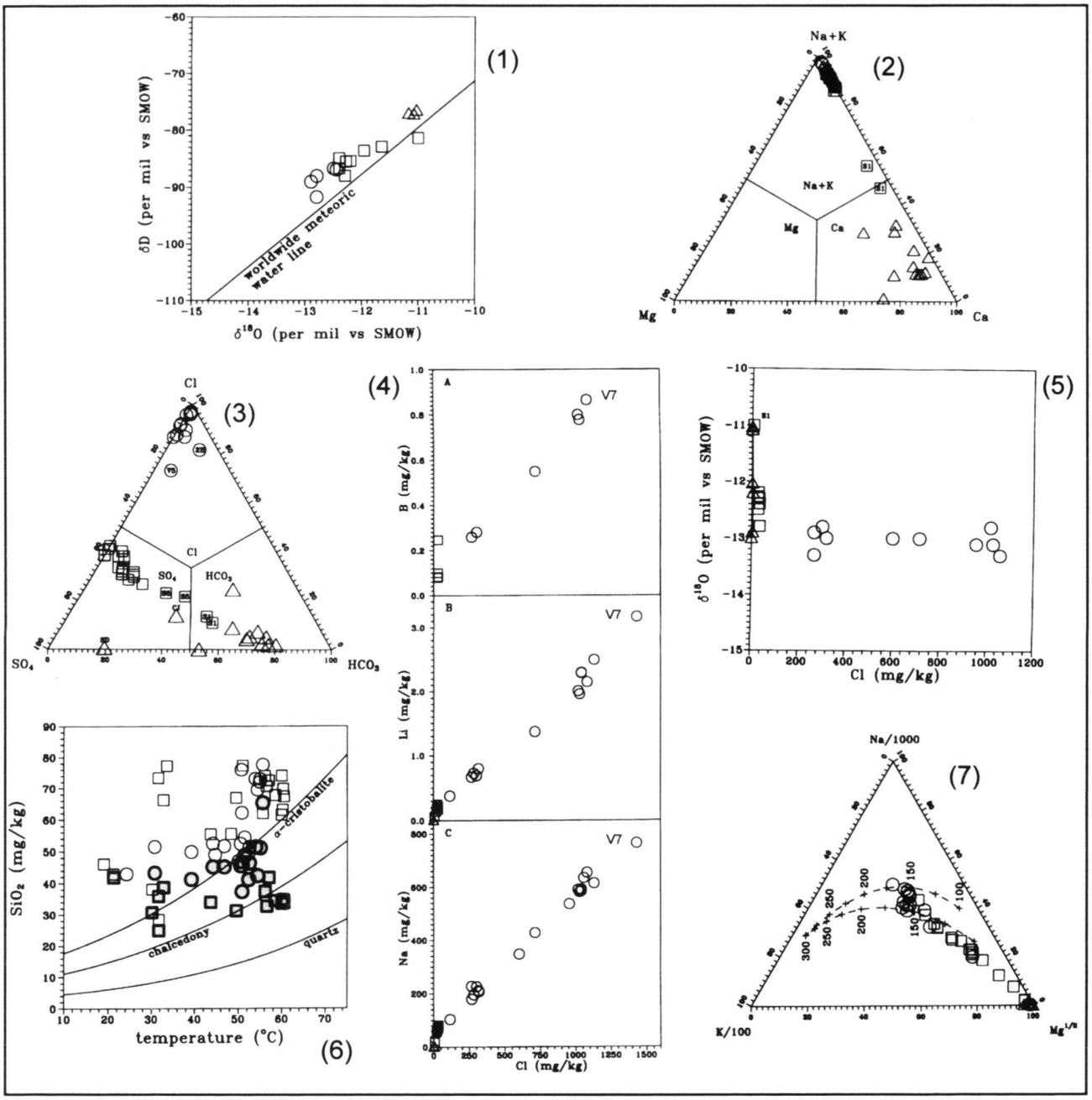

Fig. 3. Geochemical and isotopic features of thermal waters from the Argentera Massif: Circles = thermal waters of Bagni di Vinadio; squares = thermal waters of Terme di Valdieri; triangles = cold waters. Marks are the same as in Table 1.

3.1) δD vs. $\delta^{18}O$ diagram; also shown is the worldwide meteoric water line.

3.2) Relative Na^++K^+, Ca^{2+} and Mg^{2+} concentrations in equivalents.

3.3) Relative Cl^-, SO_4^{2-} and HCO_3^- concentrations in equivalents (adapted from Giggenbach, 1988).

3.4) Plots of (A) boron, (B) lithium and (C) sodium vs. chloride.

3.5) $\delta^{18}O$ values vs. Cl^- concentrations.

3.6) Plot of $SiO_{2(aq)}$ vs. temperature, reporting the concentrations of both total $SiO_{2(aq)}$ (empty symbols) and undissociated $H_4SiO_4°$ (grey symbols). The solubility curves of different silica minerals are also shown.

3.7) Relative Na^+, K^+ and $Mg^{1/2}$ concentrations on a weight basis (adapted from Giggenbach, 1988). Both full equilibrium curves are based on the K^2/Mg geothermometer of Giggenbach (1988) or on the Na/K geothermometers of Arnorsson et al. (1983) for waters in the 25-250°C range (lower curve) and Fournier (1979, upper curve).

total alkalinity of sample 3 of Michard et al. (1989; pH = 9.20), 0.970 meq/kg, is mainly explained by $H_3SiO_4^-$, with 0.574 meq/kg, and OH^-, with 0.166 meq/kg; the contribution of HCO_3^- is of 0.090 meq/kg only, and is comparable with that of HS^-, 0.089 meq/kg. Other species contributing less significantly to total alkalinity in this sample are CO_3^{2-} (0.013 meq/kg), $H_2SiO_4^{2-}$ (0.014 meq/kg), $H_2BO_3^-$(0.004 meq/kg) and $CaCO_3^\circ$ (0.004 meq/kg). The difference between total alkalinity and carbonate alkalinity is smaller at Vinadio, due to the lower pH values, but still significant. For instance sample 1D of Michard et al. (1989; pH = 8.45) has carbonate alkalinity of 0.29 meq/kg, whereas total alkalinity is 0.46 meq/kg.

Therefore, the chemical speciation has been calculated for all the thermal waters to obtain the concentration of HCO_3^- ion, which is the anion of interest, together with Cl^- and SO_4^{2-}, for the chemical classification of these waters.

The triangular plots $(Na^+ + K^+)$-Mg^{2+}-Ca^{2+} (Fig. 3.2) and HCO_3^--SO_4^{2-}-Cl^- (Fig. 3.3) show that Na^+ is the main cation in the thermal waters of both Valdieri and Vinadio, whereas the dominant anion is Cl^- at Vinadio and SO_4^{2-} at Valdieri. Relative HCO_3^- contents are very low in the thermal end-members of Valdieri and Vinadio and increase due to dilution, i.e. addition of cold, shallow groundwaters. These generally have Ca-HCO_3 composition (Tab. 1), excluding sample SD, which is a Ca-SO_4 water.

In the correlation plots between the conservative (mobile) constituents Cl^-, B and Li^+ (Fig. 3.4 a,b) all the Na-Cl waters of Vinadio distribute along a tight linear trend joining the Cl^--, B-, Li^+-rich sample V7 of Vinadio and the Cl^--, B-, Li^+-poor, Na-SO_4 waters of Valdieri.

A similar spread of points is observed in the Na^+ vs. Cl^- plot (Fig. 3.4 c). Also the $\delta^{18}O$ values, when plotted against Cl^-, define a good alignment between the Cl^--rich pole and the Cl^--poor pole (Fig. 3.5). In our opinion, these linear trends are the graphical expression of a mixing process between a low-salinity, Na-SO_4, Valdieri-type end-member and a high-salinity, Na-Cl, Vinadio(V7)-type end-member, as already suggested by Fancelli & Nuti (1978).

A different interpretation was later proposed by Michard et al. (1989), who suggested that the activities of several major and trace constituents are constrained by mineral-solution equilibria at ~115°C, under variable concentrations of Cl^-, which acts as a mobile constituent. To support this interpretation, Michard et al. (1989) pointed out the existence, in the log-log plots of dissolved species activities vs. Na^+ activity, of tight linear relationships whose slope is equal to the charge of each aqueous species. They concluded that: (1) descending waters acquire Cl^- through dissolution of the halite contained in the sedimentary rock cover; (2) subsequent mixing with Cl^-poor water produces waters of variable Cl^- concentrations; (3) these waters enter the granitic reservoirs, where they equilibrate with a number of mineral phases at ~115°C, and finally ascend towards the surface through a set of different fractures.

It should be emphasised that the interpretation of Michard et al. (1989) does not take into account the occurrence of mixing between a Vinadio (V7)-type water and a Valdieri-type water, which is clearly documented by the correlation plots between mobile constituents (see above). On the other hand, the linear trends observed by Michard et al. (1989) in log-log plots of different constituents vs. Na^+, and also our plots of Fig. 3.4–3.5, does not rule out the possible occurrence of re-equilibration after mixing between Vinadio (V7) water and Valdieri water.

For the sake of clarity, the question is: do the thermal waters of Vinadio simply originate through mixing between a Vinadio (V7)-type water and a Valdieri-type water or do some re-equilibration phenomena take place after mixing?

A way to discriminate between the simple mixing hypothesis and that of mixing plus re-equilibration is to calculate for both models the expected concentrations of pertinent chemical constituents and to compare these theoretical values with the analytical concentrations. The computation of the expected contents of mere mixtures between the Vinadio (V7) and Valdieri end-members are obviously obtained through simple mass balances. Temperatures and P_{CO2} values in the mineral-solution zone are instead needed, in addition to the contents of mobile constituents, to obtain the expected concentrations in the second model (mixing plus re-equilibration). This information can be obtained through application of suitable geothermometric and geobarometric techniques.

3.3. Geothermometry and geobarometry of thermal end-members

Due to the comparatively high pH values of the Vinadio and Valdieri thermal waters, total silica contents at outlet conditions are significantly greater than the concentrations of neutral, undissociated $SiO_{2(aq)}$, or $H_4SiO_4^\circ$. This is related to the presence of significant contents of $H_3SiO_4^-$, which are induced by high pH-values (see above). Since $SiO_{2(aq)}$ is generally involved in the hydrolysis reaction of silica minerals (quartz, chalcedony, and other phases; Fournier 1992), the concentration of this species has been calculated at outlet conditions, by means of SOLVEQ (Reed & Spycher 1984), and plotted against temperature together with total dissolved silica (Fig. 3.6). Total dissolved silica contents generally plot above the solubility curve of α-cristobalite, whereas concentrations of neutral $SiO_{2(aq)}$ are generally bracketed by the solubility curves of α-cristobalite and chalcedony. Different interpretations are possible. Based on the $SiO_{2(aq)}$ content at outlet conditions and assuming equilibrium with quartz, estimated equilibrium temperatures are in the range 105-115°C, as inferred by Michard et al. (1989). Equilibrium temperatures close to the outlet values are instead obtained admitting that thermal waters equilibrate with either α-cristobalite or chalcedony. In our opinion, silica concentrations are probably controlled by the precipitation of these silica minerals during the ascent of the thermal waters towards the surface. Anyway, in view of all these uncertainties, silica cannot be used with confidence for geothermometric purposes in this specific case. Other mineral-

solution equilibria have to be investigated to obtain indications on reservoir temperatures.

Actual achievement of mineral-solution equilibrium can be assessed by means of a Na-K-$Mg^{1/2}$ triangular plot (Fig. 3.7, Giggenbach 1988). This plot reports two curves, both representing the relative Na^+, K^+ and Mg^{2+} concentrations of geothermal waters in full equilibrium with a thermodynamically stable mineral assemblage having the composition of an average crustal rock and comprising albite, K-feldspar, muscovite, clinochlore and chalcedony. The upper full equilibrium curve includes all the aqueous solutions whose Na/K equilibrium temperature (Fournier 1979), is equal to the K^2/Mg equilibrium temperature (Giggenbach 1988). The lower curve is based on the same K^2/Mg geothermometer, but on the Na/K geothermometer of Arnorsson et al. (1983), which holds true in the 25–250°C range.

Figure 3.7 shows that: (1) some springs of both Vinadio and Valdieri plot between the two full equilibrium curves at ~150°C; (2) other thermal water discharges of both sites plot instead along a trend with Na/K ratio similar to the previous springs but with higher Mg^{2+} contents, due to either water-rock interaction and re-equilibration of Mg^{2+} at lower temperatures or mixing with shallow, Mg^{2+}-rich waters, which is likely the case of springs S1 and S5.

The P_{CO2} of the "last" mineral-solution equilibrium can be calculated from measured K^+ and Ca^{2+} contents of thermal water discharges (Giggenbach 1988). Other P_{CO2}-indicators, which are based on the HCO_3^- concentration and the K^2/Ca, Ca/Mg, HCO_3/F, and $(HCO_3)^2/SO_4$ ratios, were proposed by Chiodini et al. (1991). An initial evaluation of the equilibrium P_{CO2} for the thermal waters V7 of Vinadio (Perello 1997) and 2 of Valdieri (Michard et al. 1989), through direct application of these different P_{CO2}-indicators, was carried out by referring to the equilibrium temperature of 150°C, which is indicated by the Na-K-$Mg^{1/2}$ triangular plot (see above). Remarkably different P_{CO2} values were obtained for sample V7 of Vinadio. Possible reasons for these discrepancies are either calcite dissolution or precipitation, which are chiefly governed by either acquisition or loss of CO_2, and are described by the following reaction:

$$CaCO_3 + CO_2 + H_2O \Leftrightarrow Ca^{2+} + 2\,HCO_3^-. \qquad (2)$$

Measured Ca^{2+} and HCO_3^- concentrations were therefore corrected for variable dissolution/precipitation of calcite based on the stoichiometry of reaction (2), and inserted in the P_{CO2}-indicators listed above (Marini et al. 1998). Results are displayed versus ζ (i.e., mg of calcite dissolved or precipitated per kg of water) for sample V7 of Vinadio (Fig. 4.1a) and 2 of Valdieri (Fig. 4.1b). Figure 4.1 shows that the curves of all the P_{CO2}-indicators, apart from the $(HCO_3)^2/SO_4$ function, converge in relatively narrow ranges of P_{CO2}, ζ values for both samples. The $(HCO_3)^2/SO_4$ function overestimates the equilibrium P_{CO2} as it was derived assuming that the SO_4^{2-} concentration is fixed by anhydrite solubility, a condition which is not attained in the thermal waters of the AM (Michard et al. 1989). Equilibrium P_{CO2} values are ~0.022 bar for sample V7 of Vinadio and ~0.003 bar for sample 2 of Valdieri. These values are lower than the P_{CO2} fixed by coexistence of calcite and a Ca-Al-silicate (Giggenbach 1984), i.e., 0.055 bar at 150°C, suggesting that laumontite is stable as hydrothermal mineral in these geothermal reservoirs, while calcite forms upon CO_2 loss only. Values of ζ are close to 0 mg $CaCO_3$/kg-H_2O for sample 2 of Valdieri and approximately –12 mg $CaCO_3$/kg-H_2O for sample V7 of Vinadio, whose restored Ca^{2+} and HCO_3^- concentrations (i.e., before calcite dissolution) are 84.5 and 8.07 mg/kg, respectively.

3.4. Mere mixing or mixing plus re-equilibration ?

As discussed above, to check the hypothesis of mixing plus re-equilibration, it is necessary to calculate the equilibrium concentrations of compatible constituents at specified temperatures, P_{CO2} values and concentrations of mobile constituents. Theoretical contents of compatible constituents were calculated by means of the mineral-solution equilibrium model SOLCOMP (Guidi et al. 1990; Chiodini et al. 1991).

In the thermal waters of the Argentera Massif, Na^+, K^+, Ca^{2+}, Mg^{2+}, Al^{3+}, $SiO_{2(aq)}$, F^- and carbonate alkalinity (mainly HCO_3^-) behave as compatible ions and their activities were assumed to be constrained by the typical, hydrothermal mineral assemblage, comprising low-albite, K-feldspar, laumontite, clinochlore, muscovite, quartz, and fluorite. The HCO_3^- concentration is fixed by the specified P_{CO2} conditions.

In the thermal waters under investigation the most important mobile specie is Cl^-. Sulphate is also mobile according to Michard et al. (1989) and we accept this point of view for the purpose of the present discussion. The influence of sulphate becomes important for mixtures where the concentration of the Valdieri end-member is greater with respect to the Vinadio end-member. The contents of the generic i-th mobile constituent in any mixture are obviously constrained by a simple mass balance equation:

$$mi_M = mi_{Vi}\, x + mi_{Va}\,(1\text{-}x) \qquad (3)$$

where subscripts M, Vi and Va identify the mixture, the Vinadio end-member (m_{Cl} = 0.0405, m_{SO4} = 0.000408) and the Valdieri end-member (m_{Cl} = 0.00094, m_{SO4} = 0.000640), respectively, x is the fraction of the Vinadio end-member in the mixture and m stands for molality.

Based on the previous discussion, equilibrium temperature was taken equal to 150°C for any mixture, whereas equilibrium P_{CO2} was taken equal to 0.003 bar for a first series of mixtures and to 0.022 bar for a second set of mixtures. This implies the presence of two P_{CO2}-reservoirs that provide suitable amounts of CO_2, as soon as it is consumed through water-rock interaction, and buffers the CO_2 concentration in the equilibration zone.

Calculated concentrations of Na^+, K^+, Ca^{2+}, Mg^{2+}, F^- and carbonate alkalinity, for the model of re-equilibration after

mixing, are reported against Cl^- in Figs. 4.2-4.4. In the same figures, the expected contents upon simple mixing and the analytical values are also given. Silica and Al^{3+} are not considered since the first likely undergoes significant changes during the ascent of the thermal waters towards the surface (see above), whereas only few data are available for the second.

Figure 4.2 shows that the attainment of equilibrium with the hydrothermal paragenesis brings about a decrease of K^+ and an increase in Na^+, albeit relatively small, with respect to the contents initially fixed by mixing. Theoretical Na^+ and K^+ contents are affected by P_{CO2} at low Cl^- contents only. Most analytical Na^+ and K^+ concentrations lie close to the mixing line, whereas some samples plot between this line and the mixing plus re-equilibration curves. The evidence provided by Na^+ and K^+ is not conclusive to discriminate between simple mixing and mixing plus re-equilibration.

Equilibration with the considered hydrothermal paragenesis determines large decreases of Mg^{2+} and Ca^{2+} with respect to the concentrations initially constrained by the mixing process (Fig. 4.3). Again, theoretical Mg^{2+} and Ca^{2+} contents are influenced by P_{CO2} at low Cl^- concentrations only. Unfortunately the Mg^{2+}-content of the Valdieri end-member is poorly constrained. This fact hinders the use of Mg^{2+} for our investigation. Another process possibly affecting Ca^{2+} concentration is precipitation of calcite upon mere mixing, during the ascent of the thermal waters towards the surface (Fig. 4.3b). Theoretical Ca^{2+}-values determined by this process were computed by means of the EQ3/6 software package (Wolery 1979, 1983; Wolery & Daveler 1992). Most samples have analytical Ca^{2+} contents comparable with those expected for mixing and precipitation of calcite. Only samples 2a and 2b of Fancelli & Nuti (1978) have Ca^{2+} concentrations somewhat lower than expected, possibly because of calcium loss due to improper preservation of these samples. Accepting this explanation, Ca^{2+} provides a strong evidence against the occurrence of re-equilibration after mixing.

Carbonate alkalinity is strongly affected by equilibrium P_{CO2} at any Cl^- concentrations and remarkable changes with respect to the contents initially fixed by mixing are expected (Fig. 4.4a). Most analytical values are located between the mixing line and the mixing plus re-equilibration curves for P_{CO2}=0.22 bar, but this evidence is not conclusive, as the carbonate alkalinity of the Valdieri end-member is poorly constrained.

A significant increase in F^- content is expected upon equilibration with the hydrothermal minerals, at least for $Cl^- < 500$ mg/kg (Fig. 4.4b). Nevertheless observed F^- concentrations do not depart significantly from the mixing line, providing further evidence against the occurrence of re-equilibration after mixing, admitting that dissolved F^- is not limited by insufficient availability.

In summary, a comparison of analytical and theoretical data supports the occurrence of simple mixing between the Na-Cl, Vinadio(V7)-type end-member and the Na-SO_4, Valdieri-type end-member. Precipitation of calcite and silica minerals takes place upon mixing, probably during the ascent of the thermal waters towards the surface.

Finally it should be noted that the samples of the Vinadio thermal waters are strongly scattered in the SO_4^{2-} vs. Cl^- plot (Fig. 4.5). This spread of points is in evident contrast with the mobile behaviour of SO_4^{2-}, which was recognised by Michard et al. (1989) and accepted in the previous discussion. Vinadio samples of Fancelli & Nuti (1978) have SO_4^{2-} contents systematically higher than other samples, but similar discrepancies are not observed for Valdieri thermal waters. This exclude that the SO_4^{2-} data of Fancelli & Nuti (1978) are affected by analytical errors. It is possible, therefore, that these time-changes of SO_4^{2-} concentrations in Vinadio waters are due to variable bacterial reduction of sulphate to sulphide, a common process in thermal waters with temperatures of 30 to 100°C (e.g., Ohmoto & Goldhaber 1997 and references therein). Presently unavailable data on the isotopic composition of dissolved SO_4^{2-} are needed to substantiate this hypothesis.

4. Paleo-hydrothermal phenomena

Fossil, rock alteration phenomena are recognised in many outcrops within the AM. They are similar to the argillic and propylitic alterations, which are commonly found in many hydrothermal ore deposits. These hydrothermal alterations are usually related to H_2O-rich fluids of low to middle temperatures (Evans 1980). Rock alterations in the AM are present in two different forms: (1) diffuse alterations of great rock volumes and (2) alterations localised along shear zones, both early- and late-alpine in age.

An example of the first type is found in the AM cover succession in the Stura-Gesso area. Here rock alteration in marbles is probably related to fluids expelled during deformation at the cover/basement interface. This alteration is not described here since it does not interest directly the present work.

Many brittle to plastic shear zones in the crystalline basement (see below) are characterised by metasomatic processes and deposition of sulphide minerals (i.e. localised alterations of the second type). Hydrothermal parageneses in the brittle to plastic shear zones are usually distributed along a grid of veins. The most common hydrothermal minerals are white mica, quartz, fluorite, adularia, chlorite, calcite, tourmaline, and sulphides. At the borders of the shear zones the metasomatic alteration may extend for 10 to more than 100 cm, producing sericitization or epidotization. Often argillic tabular bodies are found along faults.

Many small sulphide ore deposits, related to these localised alterations are present inside the massif and its cover (Ruà and Lausetto mines). These mineralizations are usually constituted by galena and sphalerite with minor chalcopyrite, pyrrhotite and arsenopyrite, while the gangue is usually composed of quartz, fluorite, chlorite and calcite (Colomba 1904; Cevales 1961). Microstructural observations show that the main phase

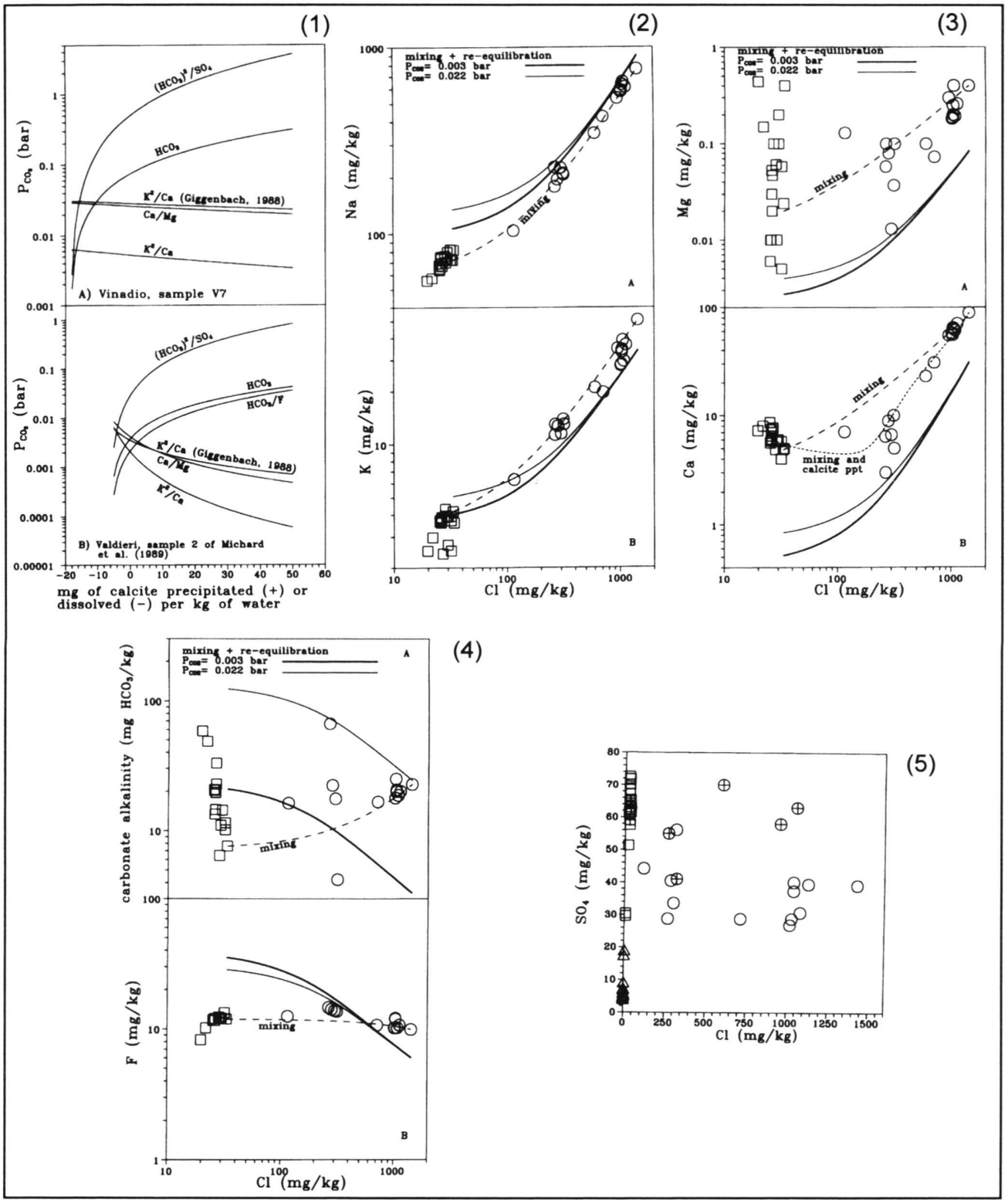

Fig. 4. Geochemical modelling of thermal waters from the Argentera Massif: symbols as in Fig. 3. See text for explanations

4.1) Plot of P_{CO2} versus the weight of calcite precipitated or dissolved (mg/kg of water) for (A) sample V7 of Bagni di Vinadio and (B) sample 2 of Terme di Valdieri (data by Michard et al. 1989).

4.2) Plots of (A) Na^+ and (B) K^+ vs. Cl^- concentrations for Bagni di Vinadio thermal waters.

4.3) Plots of (A) Mg^{2+} and (B) Ca^{2+} vs. Cl^- concentrations for Bagni di Vinadio thermal waters.

4.4) Plots of (A) carbonate alkalinity and (B) F^- vs. Cl^- concentrations for Bagni di Vinadio thermal waters.

4.5) Sulphate vs. Cl^- concentrations. The crosses identify the samples by Fancelli & Nuti (1978).

of ore deposition is usually related to a first ductile event of deformation along shear zones, probably early alpine (see below). Younger phases of ore deposition and remobilization are then related to plastic and brittle events of reactivation of late alpine age (see below).

Thermal waters circulate along the same set of faults used by old hydrothermal fluids, thus they locally leach hydrothermal rocks in addition to gneisses and metagranites.

5. Structural setting

Both the past hydrothermal alteration phenomena and the present circulation of thermal waters, with deep temperatures close to 150°C and outlet temperatures of 40–60°C, imply the presence of geological structures acting in the past and also at present as channels of high permeability. The identification of these channels (mainly fracture zones) is based on detailed structural data. These data are needed also to constrain the recent uplift and stress/strain history of the massif, which may give insights in its thermal state ultimately controlling the presence of thermal waters.

In the AM the alpine structures (folds axes and shear zones) mainly strike NW-SE (Boureau de Recherche Géologique et Minière 1977), due to the conditioning imposed from pre-alpine structural elements.

In alpine age the basement was mainly deformed in a brittle way, while the cover succession was deformed more plastically.

5.1 External sector

At the western and southern limits of the AM, the HDC is characterised by a schistosity or cleavage (S1) NE- or SW-dipping at middle to high angle (Guardia & Ivaldi 1985). These structural features may be locally related to SW-verging kilometric folds developed in anchimetamorphic conditions. Fold axes have a common NW-SE strike. S1-related folds are associated to the thrusting of the basement above the cover in ductile to brittle conditions. Thrust surfaces dip toward NE at low- to middle-angle. During thrusting the strain has been further partitioned along right-lateral, high-angle shear zones cropping out in the axial region of the massif (FM line).

The S1 is overprinted by a crenulation-cleavage (S2) still related to SW-verging folds and to SW-directed brittle thrusting of the basement above the cover (Fig. 2; Guardia & Ivaldi 1985; Bogdanoff 1986).

5.2 Internal sector

In the internal sector the alpine structures show features similar to those identified in the external sector but they have been poorly described by Authors up to now. Basement-cover relationships are complex, as reflected by the area mapped in the Stura and Gesso Valleys (Plate 1) where erosion-exhumed basement slices are tectonically pinched in the cover succession attesting a great structural complexity. The following considerations are a synthesis of detailed structural studies widely described in Perello (1997).

At the mesoscopic scale, in the cover succession of the internal AM a pervasive schistosity (S1) developed in anchimetamorphic conditions can be observed. S1 is the axial plane schistosity of tight to isoclinal folds which deforms a more or less transposed sedimentary layering called S0.

The S1 of the cover succession has no analogue inside the crystalline basement, where there is no trace of diffused schistosity development in Alpine age. The main structural features that are probably related to the S1 inside the basement are ductile greenschist facies shear zones which mainly reactivated the pre-alpine schistosity.

S1 is intersected by a younger, pervasive cleavage here called S2. S2 is structurally related with open to tight folding of the S1 at all scales. Locally the lower limbs of the S2-related folds are truncated by brittle to plastic reverse shear zones. The shear zones show brittle grain reduction processes; their thickness may vary from a few centimetres to 5–10 m. Folding and shearing are closely related and therefore they have been interpreted as the expression of the same dynamic context.

Often the brittle deformation (cataclastic flow) along the shear zones has been accompanied by hydrothermal alteration (paragraph 4) inducing sometimes ductile behaviour.

At mapping scale the basement-cover contact strikes mainly NW-SE (Fig. 2, Pl. 1) and is regionally defined by a S1-related decollement level of cargneules, but the geometry of the S1-related decollement is complicated by the presence of post-S1 structures (Pl. 1, sections A, B, C). In this internal sector two S2-related kilometric recumbent antiformal folds deform the S1 of the HDC (Plate 1). Their axes strike generally NW-SE, dipping toward the SE and the NW (Fig. 5e–f). The axial surfaces of the antiforms (S2 cleavages) dip towards the SW in the most external surveyed HDC sector and towards the NE in the most internal sector, defining a S2- to post-S2-related culmination with a SW-NE axis (Pl.1; Figs. 5a–d).

The lower limbs of the antiforms are cut by low-angle brittle, S2-related thrusts describing, like the S2, a culmination with a SW-NE axis. These thrusts enter the basement cutting the S1-related decollement and overrode the basement on the cover. The footwall of the shear zones is represented by a pile of tectonic slices separated by secondary brittle shear zones sub-parallel to the geometrically highest one (Pl. 1 map and sections). Inside the crystalline basement the strain related to plastic folding in the cover is accommodated by brittle to plastic NE-vergent reverse shears related to a NNE-SSW compression (Pl. 1, plot 8).

The thrust sheet geometry is further complicated by the presence of high-angle strike-slip faults mainly represented by two conjugate systems striking NW-SE and NE-SW or ENE-WSW. The most important system strikes NW-SE and reactivates pre-existent shear zones and the pre-alpine foliation inside the basement. These structures are widely distributed in all the studied sectors (Pl. 2 and 3), contrary to the low-angle

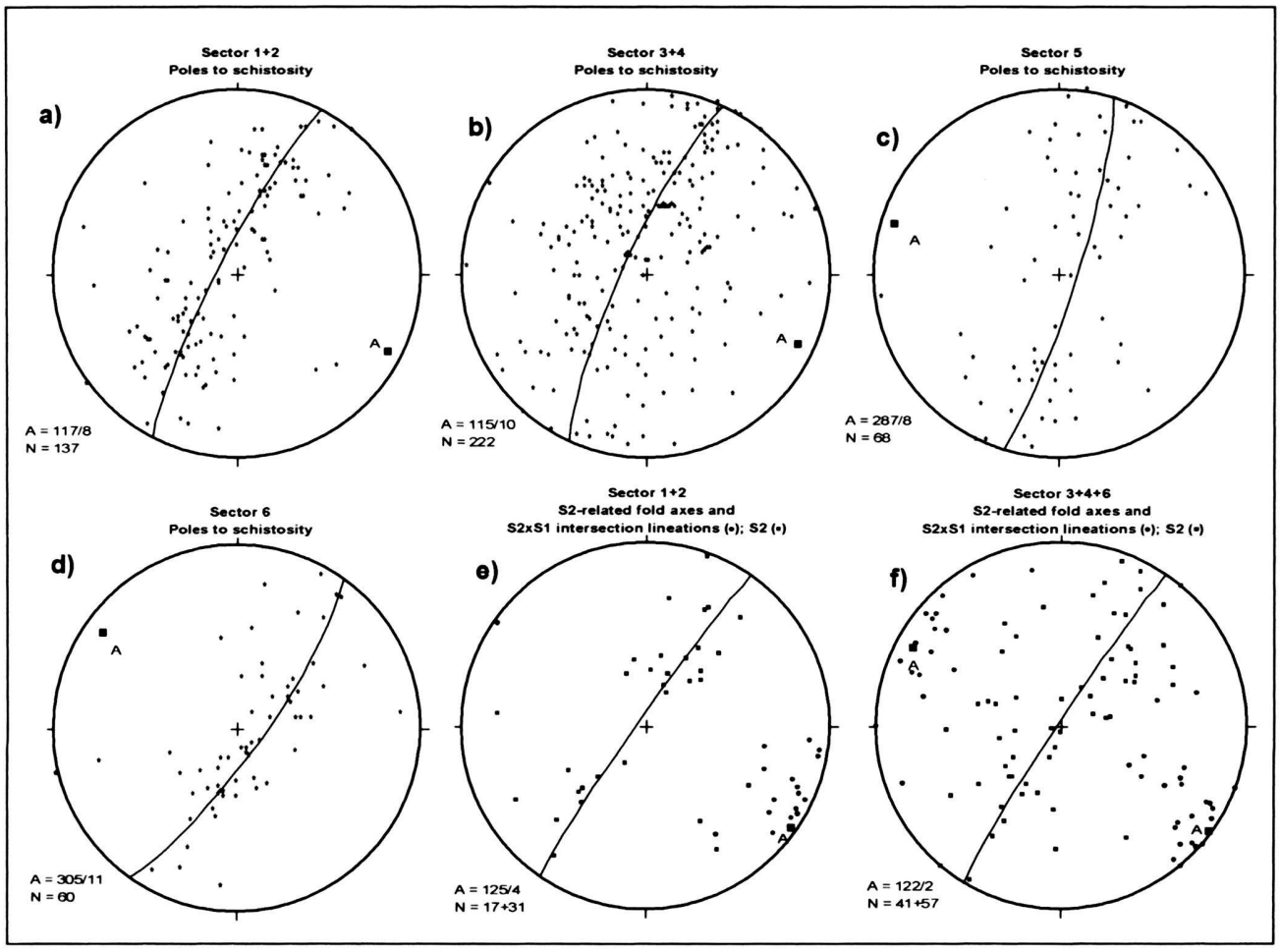

Fig. 5. Schmidt lower hemisphere plots of the schistosities, cleavages, fold axes and lineations from the Aisone-Entracque areas; plots refer to different sectors of the area mapped in Plate 1 (see map for references); N=number of measures (first number refers to the first geometric element cited in the plot title, second number to second element), A = axis of folds obtained through best fit great circle interpolation.

shear zones which are mainly concentrated near the internal cover-basement contact.

The high-angle shear zones are discontinuous faults which sometimes show en-echelon distribution (Bagni di Vinadio, Pl. 3). They may be either characterised by tectonic breccias or foliated cataclasites, or both. Their rheological behaviour strictly resembles that of the S2-related shear zones. Cataclastic flow is often associated to hydrotermally-induced plasticity, but the more plastic structures are usually strongly overprinted by still younger brittle processes. Along the most recent movement surfaces these faults show gauge affected by pervasive argillic alteration with thickness of 10-200 cm. The gauge is embedded between brecciated belts with strongly oriented structure defined by P and R surfaces (sensu Davis et al. 1999). The brecciated belts may show more or less advanced metasomatic alteration and sometimes fractures are filled by hydrothermal minerals. The thickness of the breccia and protobreccia bodies may vary from some metres to tens of metres.

Shear sense indicators suggest horizontal to oblique slip with a common component of right lateral slip for all NW-SE striking faults, and a common component of left lateral slip for all NE-SW striking faults (plots of Pl. 1, 2, 3). The oblique components, when present, mainly indicate a transpression, for the NW-SE set, and transtension for the NE-SW set. The comparison of plots 1, 2, 4, 5, 6 of Pl. 1, of plots 1, 3 of Pl. 2 and of plots 1, 4 of Pl. 3 indicates that the faults mainly accommodated a shortening in a NE-SW direction, probably related to a NNE-SSW to NE-SW principal compression axis. Anyway, in some regions the kinematic and dynamic context around the faults are different, like at stations 3 of the Stura Valley (Pl. 1), at stations 2 and 3 of Bagni di Vinadio (Pl. 3), at station 2 of Terme di Valdieri (Pl. 2). In these areas the principal shorten-

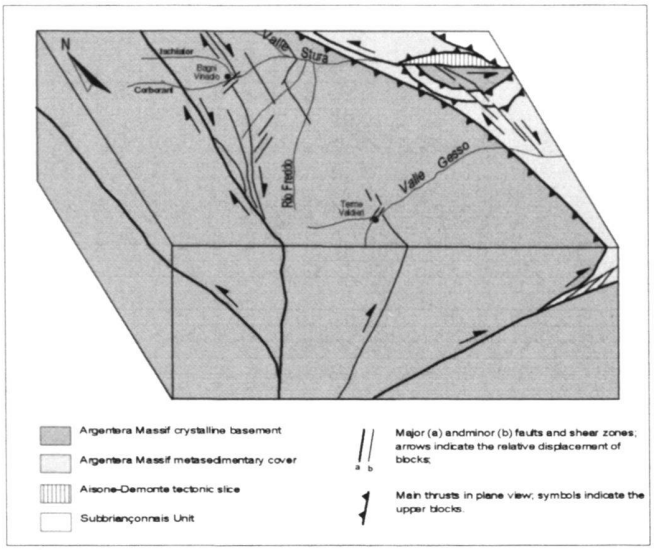

Fig. 6. Schematic block diagram of the Argentera Massif's central sector, showing the kinematic of movements along the principal shear zones in Neogene.

ing axis is rotated toward a N-S to NNW-SSE direction, and the principal compression axis is mainly N-S. This is of interest since these areas correspond to fault terminations where the thermal waters are discharged.

In the Bagni di Vinadio area a jog separates the two main brittle shear zones (Pl. 3). The step-over coincides with the bottom of the Corborant Valley, where the thermal springs are located. In the bridge area the change from the NE-SW to the N-S shortening direction is accommodated by the increase of faulting along the NE-SW directed system and the appearance of rare low- angle extensional faults dipping towards NNW (Pl. 3 plot 6).

In the Terme di Valdieri area a 150 m large, NW-SE striking cataclastic shear zone abruptly cuts off passing from the right to the left side of the Gesso Valley (Pl. 2), where the thermal waters discharge at the surface. In the termination zone the main fault splits in a great number of minor faults with similar direction.

High-angle strike slip faults have been later reactivated especially in the axial region of the massif. In the studied area the most diffuse reactivation has been observed along the northern branch of the Bagni di Vinadio junction. Shear sense indicators observed along this branch suggest that it has been reactivated as a normal fault with a NE-SW striking principal extension (Pl. 3, plot 7). Normal faulting reactivation in the axial region of the massif was reported also by Horrenberger et al. 1978). Sue et al. (1997) reported seismic data suggesting active tectonic extension along the NW-SE and NE-SW fault systems in regions nearby the AM. Thus the Bagni di Vinadio extensional reactivation could be related to recent tectonic activity. This is confirmed by our morphologic observations in the area of the fault. The left side of the Insciauda Valley, roughly corresponding to the eastern block of the reactivated fault, shows steep slopes cut by strongly eroding channels; all the glacial deposits show deep incisions near the channels. The right side, roughly corresponding to the western block, has a gentle morphology, without important erosional phenomena (Pl. 3). The intersection of the reactivated fault with the Corborant Valley corresponds to a change in morphology in the bottom of the valley. A flat alluvial plain is present upstream of the reactivated fault, whereas a deep incision in the crystalline substratum is observed downstream. These observations suggest that the northern branch of the Bagni di Vinadio junction should be still active and the eastern block is uplifting with respect to the western one.

5.3. The general geological setting of the Argentera Massif and insights in its thermal state

From a purely geometrical viewpoint the structural features newly investigated in this work and those previously surveyed (Bogdanoff 1986; Guardia & Ivaldi 1985) lead, for the AM, to a geological setting resulting mainly from the superposition of different deformational events in alpine age. The present setting closely resembles a pop-up structure, as already recognised by Fry (1989). Middle- to low-angle, S1- and S2-related thrust surfaces, striking NW-SE, border the massif both internally and externally (Fig. 6). High-angle shear zones, mainly striking NW-SE, cross the axial sector even if they often appear also in the peripheral zones. Minor, discontinuous, shear zones, striking NE-SW, are less common.

The high-angle shear zones may be interpreted as structures that partitioned the strain, which was accommodated by thrusting during the S2-related pop-up building in a transpressional context. Thrusts and strike-slip shear zones show the same rheologic behaviour, similar hydrothermal phenomena and both accommodated a NNE-SSW shortening component.

An important E-W striking, left lateral, brittle shear zone is present in the internal cover of the AM, in correspondence of the Stura Valley (Pl. 1). This important structure should represent the eastern continuation of the WNW-ESE striking "Couloir de la Stura" described by Ricou (1980), Ricou & Siddans (1986), Giglia et al. (1996). It does not enter the AM on its western continuation, since at the limit with the crystalline basement the deformation is all partitioned along NW-SE striking S2-related shear zones.

The dating of the described deformational events provides some insight into the uplift history of the massif and consequently in its thermal evolution. The S1 is an important lower age boundary for the S2-related events, which may be considered as the main recent phase of uplift. S1 is a mesoalpine feature, the related structures cut the Oligocene Gres d'Annot. The brittle S2-related deformation of the AM is thus younger than Oligocene. Fission-track apatite ages seem to point toward a progressive slow exhumation between Burdigalian and Tortonian (Bogdanoff 1991) which may represent the effect of the S2-related transpression. High-angle shear zones probably

continued to act as strike-slip faults also after the phase of active thrusting since they clearly cut thrust surfaces, but they did not cause further uplift, if not locally. In recent times the axial region of the AM has been locally affected by an extensional deformation regime, as the reactivation of older structures like the fault zone of Bagni di Vinadio and the Bersezio fault seems to attest. Therefore in recent times the axial region of the AM massif seems to sink rather than uplift, probably due to isostatic adjustments.

Contrary to other sectors of the alpine chain, where crustal blocks have been exhumed rapidly and in recent times along relatively steep discontinuities, thus originating geothermal gradients slightly higher than normal for Alpine areas (e.g., the Lepontine Dome region; Steck & Hunziker, 1994 and references therein), the AM has been exhumed progressively along low- to middle-angle surfaces. Furthermore its exhumation is older than in regions of anomalous geothermal gradient. This uplift history suggests that in the AM the geothermal gradient should be relatively low, if it is not influenced by other factors apart from uplift, which are not to be supposed in the study area. This inference is confirmed by the temperatures measured in the exploratory Ciriegia tunnel, which was excavated in the valley of Terme di Valdieri (Bortolami & Grasso 1969). The maximum depth of the Ciriegia tunnel is close to 700 m and maximum temperatures are 19–20°C. Admitting that the annual average air temperature at the surface is 5–7°C at the tunnel elevation (Regione Piemonte, 1998), the apparent geothermal gradient is of 19–21°C/Km. Even considering a strong influence of topography it seems unlikely that this gradient can be greater than 25°C/km. Due to this relatively low geothermal gradient, the reason for thermalism in the AM has to be found in other phenomena than the recent uplift, such as, for example, the present tectonic activity along the old strike-slip shear zones that have been locally reactivated as normal faults, as discussed in the next section.

6. Discussion

The structural and geochemical data presented in the previous sections allow the construction of a conceptual model for the thermal circuits of the AM.

Geochemical data indicate that at Terme di Valdieri the thermal springs discharge a pure Na-SO_4 end-member, sometimes diluted by addition of cold shallow waters, while at Bagni di Vinadio the thermal springs discharge mixtures made up of Na-Cl, Vinadio(V7)-type end-member and the Na-SO_4, Valdieri-type end-member. Mixing takes probably place during the ascent of the thermal waters towards the surface and induces variable precipitation of calcite and silica minerals.

All the thermal waters are Na^+-rich, which is a common feature of waters circulating in gneissic and granitic massifs (Michard et al. 1989). However, the large compositional variability of Vinadio thermal springs is a peculiarity of the AM.

Most thermal waters of the AM have deep (geothermometric) temperatures close to 150°C, which is one of the highest values for the thermal waters of the Alpine chain. In addition these thermal waters plot close to the worldwide meteoric line, indicating a pure meteoric origin.

These thermal waters are able to reach the surface due to specific conditions, which are probably the fortuitous combination of favourable geologic and morphologic factors. Both at Terme di Valdieri and Bagni di Vinadio, the thermal waters reach the surface in the bottoms of the valleys, a short distance upstream of the intersection between the valleys and NW-SE striking cataclastic shear zones. Moreover, mapped geological data and structural analysis demonstrate that in both areas the shear zones intersect the valleys in coincidence with either a lateral termination, like at Terme di Valdieri, or a step-over between two en-echelon brittle shear zones, like at Bagni di Vinadio.

It has been demonstrated (e.g. Sibson 1987) that jog structures like those of Bagni di Vinadio represent preferential regions of ore deposition related to hydrothermal activity, thus confirming their importance in fluid circulation.

The thermal water outflows of Bagni di Vinadio and Terme di Valdieri must be related to the presence of permeability changes at jog and tip regions, but also, more generally, near the cataclastic shear zones. The permeability of cataclastic shear zones in crystalline rocks is hard to define. It has been demonstrated that permeability is very high, not inside the shear zone, but close to its borders (Wallace & Morris 1986; Evans et al. 1997). In cataclastic shear zones permeability is usually greatly increased parallel to the fault plane, since in that directions the tortuosity of the flux is highly decreased (Arch & Maltman 1990; Moore et al. 1990). Conversely permeability is greatly decreased in a transversal direction with respect to the shear zone surface, due to the lack of structural discontinuities oriented in this direction. Evans et al. (1997) recognised, in some shear zones of granitic complexes, a zoned structure made up of a low-permeability core, mainly composed of fine-grained cataclasites and gauge, and lateral damaged zones of high permeability, mainly composed of coarse-grained tectonic breccias. This structure strictly resembles that observed in the cataclastic shear zones of the studied region (see above). This permeability distribution in and nearby the cataclastic shear zones causes them to act as barriers for waters flowing in a transverse direction and as conduits for waters flowing in a direction parallel to the fault plane. For the particular case of the AM, waters infiltrating in the axial region of high elevations, probably tend to migrate towards the peripheral regions where the hydrostatic load is lower. Their migration is therefore transversal with respect to major NW-SE oriented shears which oppose to migration and cause the upflow of waters along the high permeability belts parallel to them. Obviously the preferential upflow regions are the step-overs, where more structure converge (Fig. 6a), and the tips, where structures end and the permeability dramatically change from high to very low values. The fact that the thermal waters are discharged upstream the shear zones is probably related to the permeability distribution; the higher permeability is met not

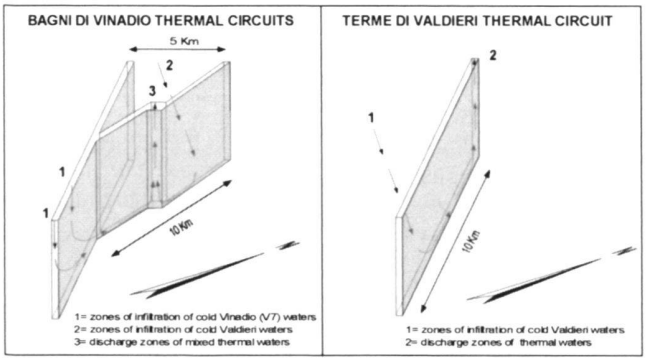

Fig. 7. Circulation schemes for the thermal waters of the Argentera Massif; figures represent the simplified geometry of the high angle shear zones cross-cutting the crystalline basement where the thermal waters infiltrate and circulate. Arrows indicate the presumed pathway of the waters.

inside the shear zone but at its border some tens of metres apart from the more deformed belt (see previous considerations).

Also the relatively high temperatures at depth of these thermal waters (~150°C) require an explanation, especially because they are not related to anomalous geothermal gradients. Since in the AM the geothermal gradient should be close to 25°C/km, temperatures of ~150°C are reached at depths of 5–6 km below the topographic surface. As fracture permeability decreases with the pressure increase (Evans et al. 1997) and thus with lithostatic load, at 5 km depth it is probably 4–5 orders of magnitude lower than at the surface, thus preventing significant water circulation. However, favourable in situ stress conditions increase fracture permeability of 2–3 orders of magnitude (Banks et al. 1996). Such conditions are likely present in the AM, due to the recent stress field (paragraph 5.2; NE-SW extensional stresses acting along the NW-SE striking faults), allowing the development of geothermal reservoirs at greater depths than in other sectors of the Alps.

A last point which remains to be explained is the compositional difference between the two geothermal end-members, which is not justified by the homogeneous mineralogical composition of the rocks of the AM. In particular, there is no general consensus on the source of Cl^-, which is present in comparatively high concentrations in the Bagni di Vinadio end-member.

Michard et al. (1989) proposed that Cl^- and Na^+ come from halite dissolution. This hypothesis has to be rejected since no halite is known to be present in the HDC. However, even admitting that Cl^- comes from dissolution of the halite contained in the rocks of the cover succession, thermal waters would be expected to be close to saturation, at reservoir temperature, with respect to anhydrite, which is a common phase in alpine evaporite horizons. This is not the case for the Argentera waters, which are strongly undersaturated with respect to anhydrite. Although bacterial reduction of sulphate to sulphide might have caused a significant decrease of the sulphate contents, thus determining the state of undersaturation with respect to anhydrite, it is difficult to accept a decrease from 1350 mg/kg (the saturation value at 150°C admitting saturation with respect to anhydrite and calcite, calculated by means of SOLVEQ (Reed & Spycher 1984) to the observed ~40 mg/kg for the Vinadio end-member.

Bortolami et al. (1984) proposed instead that the high Cl^- contents of Bagni di Vinadio waters are related to mixing at depth of descending meteoric waters with connate brines coming from the Po Valley through injection inside the massif along important tectonic lineaments. Also this hypothesis has to be re-discussed on geologic ground, since all the recent cataclastic shear zones have NW-SE direction, i.e. they are transversal to the presumed direction of migration of the Po Valley brines. Even the E-W striking "Couloir de la Stura" does not seem to enter the massif. To be injected inside the massif, these brines should pass transversally through all the shear zones of the thrust system bordering the massif in the Stura and Gesso Valley. This is not realistic because the permeability of this system in a transversal direction is very low.

We alternatively propose that the main Cl^- source for the thermal waters of the AM is represented by the phyllosilicates and the fluid inclusions contained in the crystalline rocks of the massif. Chloride can replace the OH^- group in the phyllosilicates (Edmunds et al., 1984), and is very abundant in fluid inclusions, since their major solute is generally NaCl (Roedder and Bodnar 1997). Though it is a trace element in rocks, it can concentrate in waters since it is a very mobile anion, and when it enters the solutions it is hardly removed, unless saturation with respect to halite is attained. For this reason Cl^- contents in groundwaters of meteoric origin generally increase with the circulation times, that is with the time of water-rock interaction. In our opinion, the different Cl^- and Na^+ contents of the two end-members of the AM reflect the different Cl^- and Na^+ contents of the rocks where they circulated. The Valdieri end-member, which is present at both sites, and thus seems to indicate the normal composition of waters circulating in the massif, probably originate through leaching of widespread granitic and migmatitic rocks with relatively low Cl^- and Na^+ contents. On the contrary, the Vinadio end-member, which represents a local anomaly, probably originates through leaching of cataclastic hydrotermalized rocks, which are diffused along the NW-SE faults (paragraph 5.2). These rocks commonly show anomalously high contents in phyllosilicate minerals, due to hydration reactions. Moreover, and even more remarkably, they are very rich in fluid inclusions, which are diffused features related to hydrothermal deposition (Evans 1980).

7. Conclusions

Based on the above discussion, we propose the following conceptual circulation model for the thermal waters of the AM (Fig. 7).

At Terme di Valdieri the descending meteoric waters enter the granitic-migmatitic reservoir, where they equilibrate at

temperatures close to 150°C, acquiring a Na-SO_4 composition. These thermal waters ascend quickly through a brittle shear zone and discharge at the surface where the tip point of this tectonic element intersects the bottom of the valley.

At Bagni di Vinadio, the Na-SO_4 end-member experiences a circulation history similar to that of the Valdieri thermal waters. The other end-member, of Na-Cl composition, originates through circulation of meteoric waters into the peculiar deep reservoir represented by the FM cataclastic rocks rich in hydrothermal ore deposits. The high Cl^- concentrations are probably related to the leaching of metasomatic rocks rich in phyllosilicates and mineralizations with Na-Cl fluid inclusions. This Na-Cl end-member upflows along a branch of the main discontinuity which ends in the step-over of Bagni di Vinadio. Along their route to the surface, Na-SO_4 and Na-Cl waters mix in variable proportion triggering precipitation of calcite and silica minerals.

Acknowledgements

The authors want to thank Sabrina Pastorelli, both for the support in the acquisition of analytical data and for the discussions concerning the geothermal aspects. Structural aspects have been greatly improved by field excursions and discussions with Fabrizio Piana. Our thanks goes also to Prof. L. Rybach and to an anonymous reviewer for their helpful comments to the first version of this manuscript.

REFERENCES

ANGELIER, J. & MECHLER, P. 1977: Sur une méthode graphique de recherche des contraintes principales également utilisable en tectonique et en séismologie: la méthode des diédres droits. Bull. Soc. Géol. France (7), 19/6, 1309–1318.

ARCH, J. & MALTMAN, A. 1990: Anisotropic permeability and tortuosity in deformed wet sediments. J. Geoph. Res. 95, 9035–9045.

ARNORSSON, S., GUNNLAUGSSON, E., SVAVARSSON, H. 1983: The chemistry of geothermal waters in Iceland. III. Chemical geothermometry in geothermal investigations. Geoch. Cosmoch. Acta 47, 567–577.

BANKS, D., ODLING, N.E., SKARPHAGEN, H., ROHR-TORP, E. 1996: Permeability and stress in crystalline rocks. Terra Nova 8, 223–235.

BOGDANOFF, S. 1986: Evolution de la partie occidentale du Massif cristallin externe de l'Argentera. Place dans l'arc Alpin. Géol. France 4, 433-453.

– 1991: Evolution du Massif de l'Argentera. Boll. Mus. Reg. SCI. Nat. 9 (1) 23–43.

BORTOLAMI , G. & GRASSO, F. 1969: Osservazioni geologico-applicative sul cuniclo d'assaggio del Traforo del Ciriegia e considerazioni sull'intero tracciato, Atti 1° Conv. Int. „Problemi tecnici nella costurzione di gallerie", 111–126.

BORTOLAMI, G., OLIVERO, G.F., ZUPPI, G.M. 1984: Sistemi idrici profondi, geotermali e freddi in Piemonte e Valle d'Aosta: Mem. Soc. Geol. It. 29, 171–185.

Bureau de Recherche Géologique et Minière 1977: Carte géologique de la France a 1:50.000, Feuille "Larche" XXXVI-39.

CEVALES, G. 1961: Il giacimento piombo-zincifero di Ruà presso le Terme di Vinadio, Valle Stura di Demonte, Cuneo. Ind. Miner. 12, 677–684.

CHIODINI, G., CIONI, R., GUIDI, M., MARINI L. 1991: Chemical geothermometry and geobarometry in hydrothermal aqueous solutions: a theoretical investigation based on a mineral-solution equilibrium model. Geoch. Cosmoch. Acta 55, 2709–2727.

CLARK, S.P. & NIBLETT, E.R. 1956: Terrestrial heat flow in the swiss Alps: montly Notices of the Royal Astr. Soc. Geoph. Supp. 7–4, 176–195.

COLOMBA, L. 1904: Cenni preliminari sui minerali del Lausetto (valli del Gesso). Boll Soc. Geol. It. 23 (3), 392–397.

COMPAGNONI, R., LOMBARDO, B., PRATO, R. 1974: Andalousite et sillimanite aux contacts du granite central de l'Argentera (Alpes Maritimes). Soc. It. Min; Petr. 30 (1), 35–54.

DAVIS, G.H., BUMP, A.P., GARCÌA, P.E., AHLGREN, S.G. 1999: Conjugate Riedel deformation band shear zones. Journ. Struct. Geol. 22, 169–190.

DAZY, J., DRAY, M., JUSSERAND, C., PASQUALOTTO, M., ZUPPI, G.M. 1987: Caracterisation isotopique des eaux thermominerales des Alpes du nord Franco-Italiennes. „Isotope techniques in water resources development" IAEA Ed., Vienna, 24 pp.

EDMUNDS, W.M., ANDREWS, J.N., BURGESS, W.G., KAY, R.L.F., LEE, D.J. 1984: The evolution of saline and thermal groundwaters in the Carnmenellis granite. Min. Magazine 48, 407–424.

EVANS, A.M., 1980: An Introduction to ore geology.

EVANS, J.P., FORSTER, C.B., GODDARD, J.V., 1997: Permeability of fault-related rocks and implications for hydrulic structure of fault zones. J. Struct. Geol. 19/11, 1393–1404.

FANCELLI, R. & NUTI, S. 1978: Studio geochimico delle sorgenti termali del Massiccio cristallino dell'Argentera (Alpi Marittime). Boll. Soc. Geol. It. 97, 115–130.

FAURE-MURET, A. 1955: Etudes géologiques sur le Massif de l'Argentera-Mercantour et ses enveloppes sédimentaires. Mem. Carte Géol. France, 336 pp.

FERRARA, G. & MALARODA, R. 1969: Radiometric age of granitic rocks from the Argentera Massif (Maritime Alps). Boll. Soc. Geol. It. 88, 311–320.

FOURNIER, R.O. 1979: A revised equation for the Na/K geothermometer. Geotherm. Res. Counc. Trans. 3, 221–224.

– 1992: Water geothermometers applied to geothermal energy. In „Applications of geochemistry in geothermal reservoir development, United Nations Institute Trainig & Research Ed. 37–69.

FRY, N. 1989: Southwestward thrusting and tectonics of the western Alps. In Coward, M., Dietrich, D., Park, R.G. (eds.) „Alpine Tectonics". Geol. Soc. Spes. Pub. 45, 83–111.

GIGGENBACH W. F. 1984: Mass transfer in hydrothermal alteration systems. A conceptual approach. Geochim. Cosmochim. Acta 48, 2693–2711.

– 1988: Geothermal solute equilibria. Derivation of Na-K-Mg-Ca geoindicators. Geoch. Cosmoch. Acta 52, 2749–2765.

– 1992: Isotopic composition of geothermal water and steam discharges. In "Application of Geochemistry in Geothermal Reservoir Development" (D'Amore F., co-ordinator). Unitar / UNDP Center on Small Energy Resources, Rome, 253–273.

GUARDIA, P. & IVALDI, J.P. 1985: Les déformations schistogénes du tégument de l'Argentera (Alpes-Maritimes): description, genése et chronologie relative dans le cadre géodinamyque des Alpes sud-occidentales. Bull. Soc. Géol. France 8/1, 353–362.

GUIDI M., MARINI L., SCANDIFFIO G., CIONI R. 1990: Chemical geothermometry in hydrothermal aqueous solutions: the influence of ion complexing. Geothermics 19, 415–441.

GIGLIA, G., CAPPONI, G., CRISPINI, L., PIAZZA, M. 1996: Dynamics and seismotectonics of the West-Alpine arc. Tectonophys, 267, 143–175.

HORRENBERGER, J.C., MICHARD, A., WERNER, P. 1978: Le couloir de décrochement de Bersezio en Haute-Stura, Alpes externes Italie. Structure de compression sub-méridienne. Sci. Geol. Bull. 31, 15–20.

HUBBARD, M. & MANCKTELOW, N.S. 1992: Lateral displacement during Neogene convergence in the western and central Alps. Geology 20, 943–946.

LAUBSCHER, H. 1991: The arc of the western Alps today. Ecl. Geol. Helv. 84/3, 631–659.

MALARODA, R., CARRARO, F., DAL PIAZ, G.V., FRANCESCHETTI, B., STURANI, C., ZANELLA, E. 1970: Carta geologica del Massiccio dell'Argentera alla scala 1:50.000 e note illustrative. Mem. Soc. Geol. It. 9, 557–663.

MANCKTELOW, N. 1985: The Simplon Line: a major displacement zone in the western Lepontine Alps. Ecl. Geol. Helv. 78/1, 73–96.

MARINI, L., CHIODINI, G., CIONI, R. 1986: New geothermometers for carbonate-evaporite geothermal reservoirs. Geothermics, 15/1, 77–86.

MARINI L., CIONI R., GUIDI M. 1998: Water chemistry of San Marcos area, Guatemala. Geothermics 27, 331–360.

MICHARD, G., GRIMAUD, D., D'AMORE, F., FANCELLI, R. 1989: Influence of mobile ion concentrations on the chemical composition of geothermal waters in granitic areas, example of hot springs from Piemonte (Italy). Geothermics 18 (5/6), 729–741.

MOORE, J.C., ORANGE, D., KULM, L.D. 1990: Interrelationships of fluid venting and structural evolution: Alvin observations from the frontal accretionary prism, Oregon. Jour. Geoph. Res. 95/B6, 8795–8808.

OHMOTO H. & GOLDHABER M.B. (1997) Sulfur and carbon isotopes. In "Geochemistry of hydrothermal ore deposits", 3d ed. (Ed. by H.L. BARNES), Chapter 11, 517–611. J.Wiley, New York.

PASTORELLI S., MARINI L., HUNZIKER J.C. 1999: Water chemistry and isotope composition of the Acquarossa thermal system, Ticino, Switzerland. Geothermics 28, 75–93.

PEARSON F.J. & TRUESDELL A.H. 1978: Tritium in the waters of Yellowstone National Park. U.S. Geological Survey Open-file Report 78–701.

PERELLO, P. 1997: interazioni tra strutture tettoniche, fenomeni di sollevamento rapido recente e manifestazioni geotermiche a bassa entalpia nelle Alpi occidentali. Studio di quattro località tipo: Settore ossolano, Alta Valle d'Aosta, Settore vallesano, Massiccio dell'Argentera. Tesi dottorato Dip. Scienze della Terra, Univ. Torino (Italia), 200pp.

PERELLO, P., PIANA, F., MARTINOTTI G. 1999: Neo-Alpine structural features at the boundary between the Penninic and Helvetic domains (Pré Saint Didiér – Entrèves, Aosta Valley, Italy). Ecl. Geol. Helv. 92, 347–359

REED M.H., SPYCHER N.F. 1984: Calculation of pH and mineral equilibria in hydrothermal waters with application to geothermometry and studies of boiling and dilution. Geochim. Cosmochim. Acta 48, 1479–1492.

RICOU, L.E. 1980: La zone Subbriançonnaise des Alpes occidentales interprétée comme la trace d'un ample décrochement senestre subméridien. C.R. Acad. Sci. (Paris), 292, 1305–1308.

RICOU, L.E. & SIDDANS, A.W.B. 1986: Collision tectonics in the Western Alps. In "Collision Tectonics", (Ed. by COWARD M.P. & RIES A.C, Geol. Soc. Spec. Pub. 19, 229–244.

ROEDDER, E. & BODNAR, R.J. 1997: Fluid inclusion studies of hydrothermal ore deposits. In: Geochemistry of hydrothermal ore deposits, (H.L. Barnes), third edition, Wiley, 657-697.

ROZANSKI K., ARAGUAS-ARAGUAS L., GONFIANTINI R. 1993: Isotopic patterns in modern global precipitation. In: Climate Change in Continental Isotopic Records. Geophysical Monograph 78, American Geophysical Union, 1–36.

RYBACH L. 1995: Thermal waters in deep Alpine tunnels. Geothermics 24, 631–637.

SEWARD, D. & MANCKTELOW, N.S. 1994: Neogene kinematics of the central and western Alps: evidence from fission-track dating. Geology 22, 803–806.

SIBSON R.H. 1987: Earthquake rupturing as a mineralizing agent in hydrothermal systems. Geology 15, 701–704.

STECK, A. 1990: Une carte des zones de cisaillement ductile des Alpes centrales. Ecl. Geol. Helv. 83/3), 603–627.

STECK, A. & HUNZIKER, J.C. 1994: The Tertiary structural and thermal evolution of the central Alps -compressional and extensional structures in an orogenic belt. Tectonophys 238, 26 pp.

STURANI, C. 1962: Il complesso sedimentario autoctono all'estremo nord-occidentale del Massiccio dell'Argentera (Alpi Marittme). Mem. Ist. geol. Min. Univ. Padova 22, 178 pp.

– 1963: La couverture sédimentaire de l'Argentera-Mercantour dans le secteur compris entre les Barricate et Vinadio. Trav. Lab. Geol. Grenoble 39, 83–124.

SUE, C., MARTINOD, J., TRICART, P., GAMOND, J.F., THOUVENOT, F., FRECHET, J., MARINIER, D 1997: Are internal alpine zones expanding? New geodetic evidences. Proceed of the 3[d] Workshop on alpine geological studies, Oropa-Biella (Italy), Quaderni Geodin. alpina Quaternaria 4, 127.

VUATAZ, F.D. 1982: Hydrogéologie, géochimie et géothermie des eaux thermales de Suisse et des régions alpines limitrophes. Mat. Géol. Suisse – Hydrol. 29. Soc. Helv. Sc. Nat. Pub., 174pp.

WALLACE, E.E. & MORRIS, H.T. 1986: Characteristics of faults and shear zones in deep mines. Pure and Appl. Geoph. 124, 107–126.

WOLERY T. 1979: Calculation of chemical equilibrium between aqueous solutions and minerals: the EQ3/6 software package. Report UCRL-52658. Lawrence Livermore National Laboratory, Livermore.

– 1983: EQ3NR: A computer program for geochemical aqueous speciation-solubility calculations. User's guide and documentation. Report UCRL-53414. Lawrence Livermore National Laboratory, Livermore.

WOLERY T. & DAVELER 1992: EQ6: A computer program for reaction path modeling of aqueous geochemical systems: Theoretical manual, user's guide and related documentation. Report UCRL-53788. Lawrence Livermore National Laboratory, Livermore.

Manuscript received November 1, 1999
Revision accepted December 28, 2000

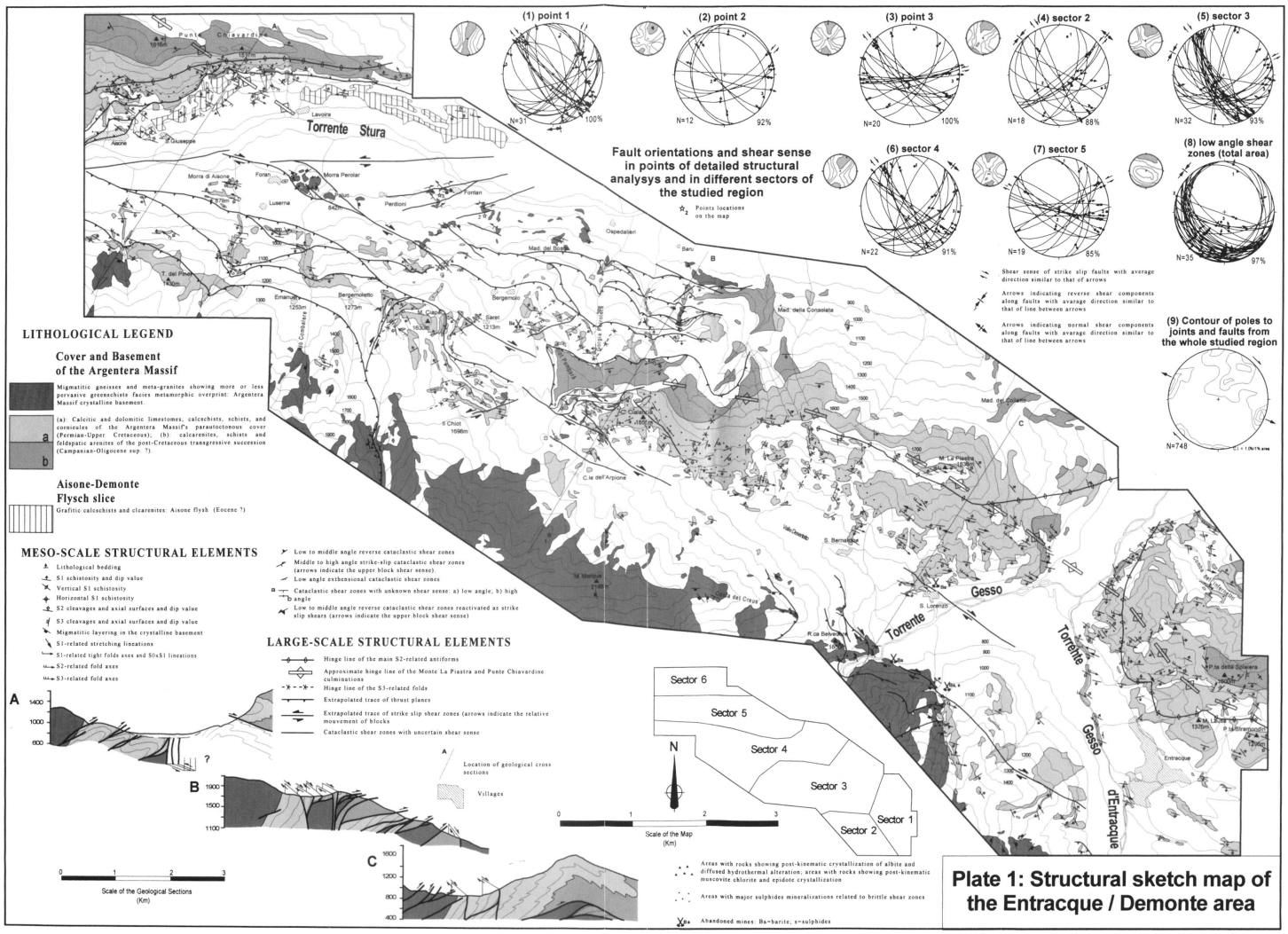

Plate 1. Structural sketch map of the Entracque/Demonte area. Included plots are equal area Schmidt diagrams. Big plots show great circles of measured faults together with poles to strine measured on faults: arrows indicate the shear sense of upper blocks; 1>2>3 = finite strain axes deduced form the Angelier & Mechler (1977) method; N=number of faults, %=percentage of faults fitting the solution of the Angelier & Mechler (1977) method. Little plots are P-dihedra contours of faults fitting the Angelier & Mechler (1977) method where have been evidenced in black and grey respectively the first and second classes with higher density: these plots suggest the possible regions where lays the principal compressive stress direction during deformation. Also plotted is a contour of poles to measured joints.

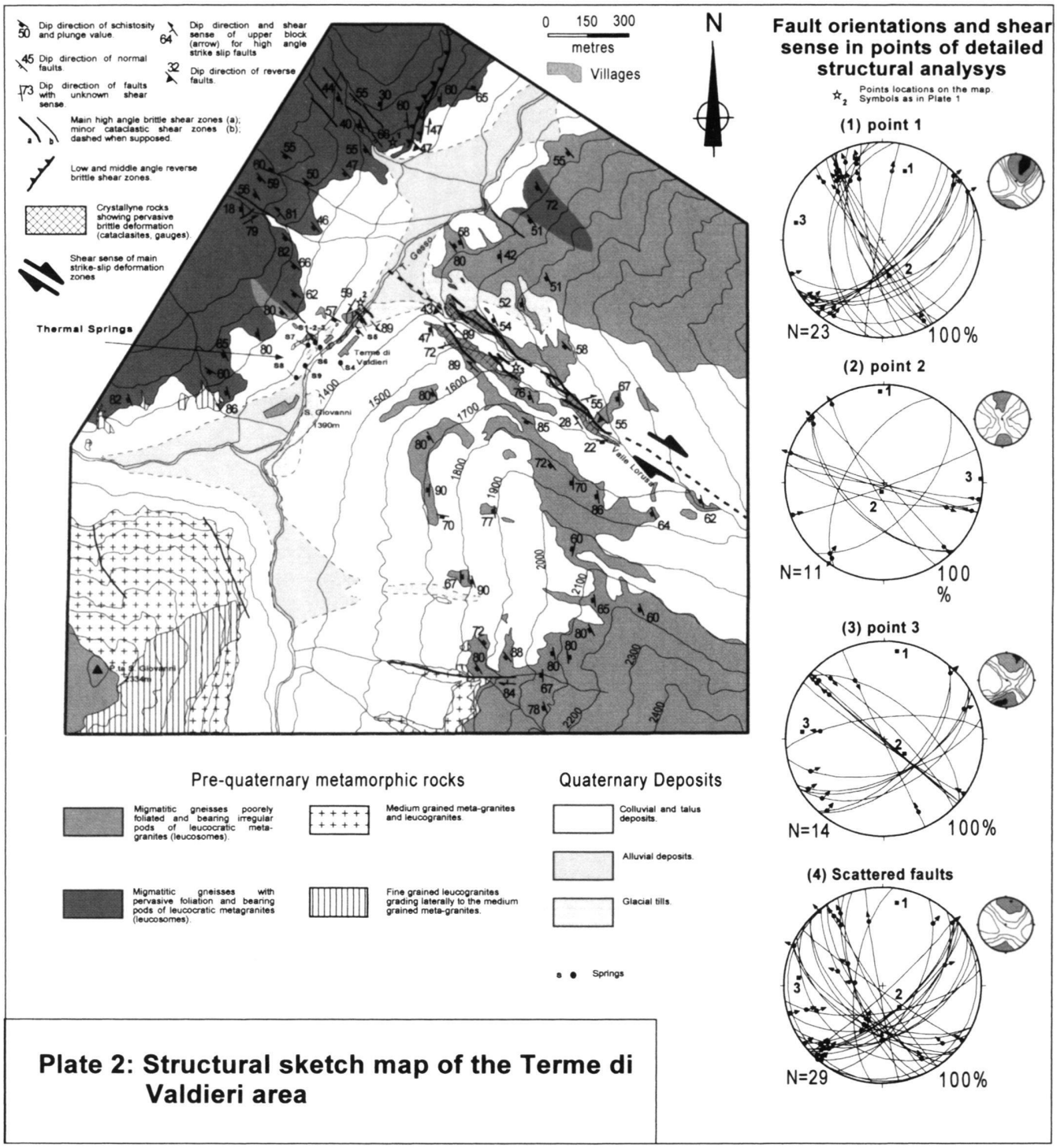

Plate 2: Structural sketch map of the Terme di Valdieri area

Plate 2. Structural Sketch map of the Terme di Valdieri Area. Included plots are equal area Schmidt diagrams. See Plate 1 for symbols in plots.

Plate 3. Structural Sketch map of the Bagni di Vinadio Area. Included plots are equal area Schmidt diagrams. See Plate 1 for symbols in plots.

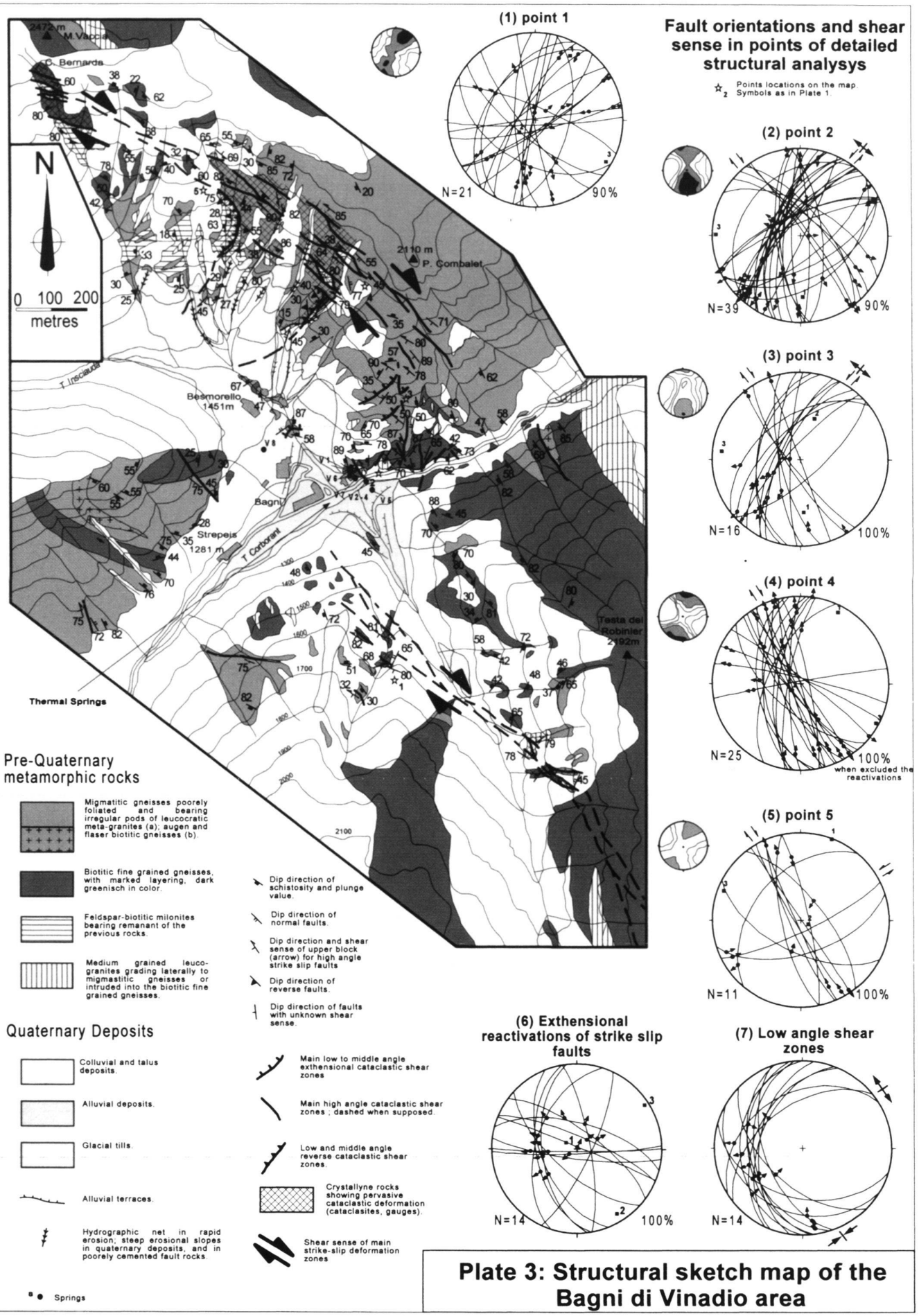

Fault orientations and shear sense in points of detailed structural analysys

☆2 Points locations on the map. Symbols as in Plate 1.

Pre-Quaternary metamorphic rocks

Migmatitic gneisses poorely foliated and bearing irregular pods of leucocratic meta-granites (a); augen and flaser biotitic gneisses (b).

Biotitic fine grained gneisses, with marked layering, dark greenisch in color.

Feldspar-biotitic milonites bearing remanant of the previous rocks.

Medium grained leuco-granites grading laterally to migmastitic gneisses or intruded into the biotitic fine grained gneisses.

Dip direction of schistosity and plunge value.

Dip direction of normal faults.

Dip direction and shear sense of upper block (arrow) for high angle strike slip faults.

Dip direction of reverse faults.

Dip direction of faults with unknown shear sense.

Quaternary Deposits

Colluvial and talus deposits.

Alluvial deposits.

Glacial tills.

Alluvial terraces.

Hydrographic net in rapid erosion; steep erosional slopes in quaternary deposits, and in poorely cemented fault rocks.

Springs

Main low to middle angle exthensional cataclastic shear zones

Main high angle cataclastic shear zones ; dashed when supposed.

Low and middle angle reverse cataclastic shear zones.

Crystallyne rocks showing pervasive cataclastic deformation (cataclasites, gauges).

Shear sense of main strike-slip deformation zones

Plate 3: Structural sketch map of the Bagni di Vinadio area